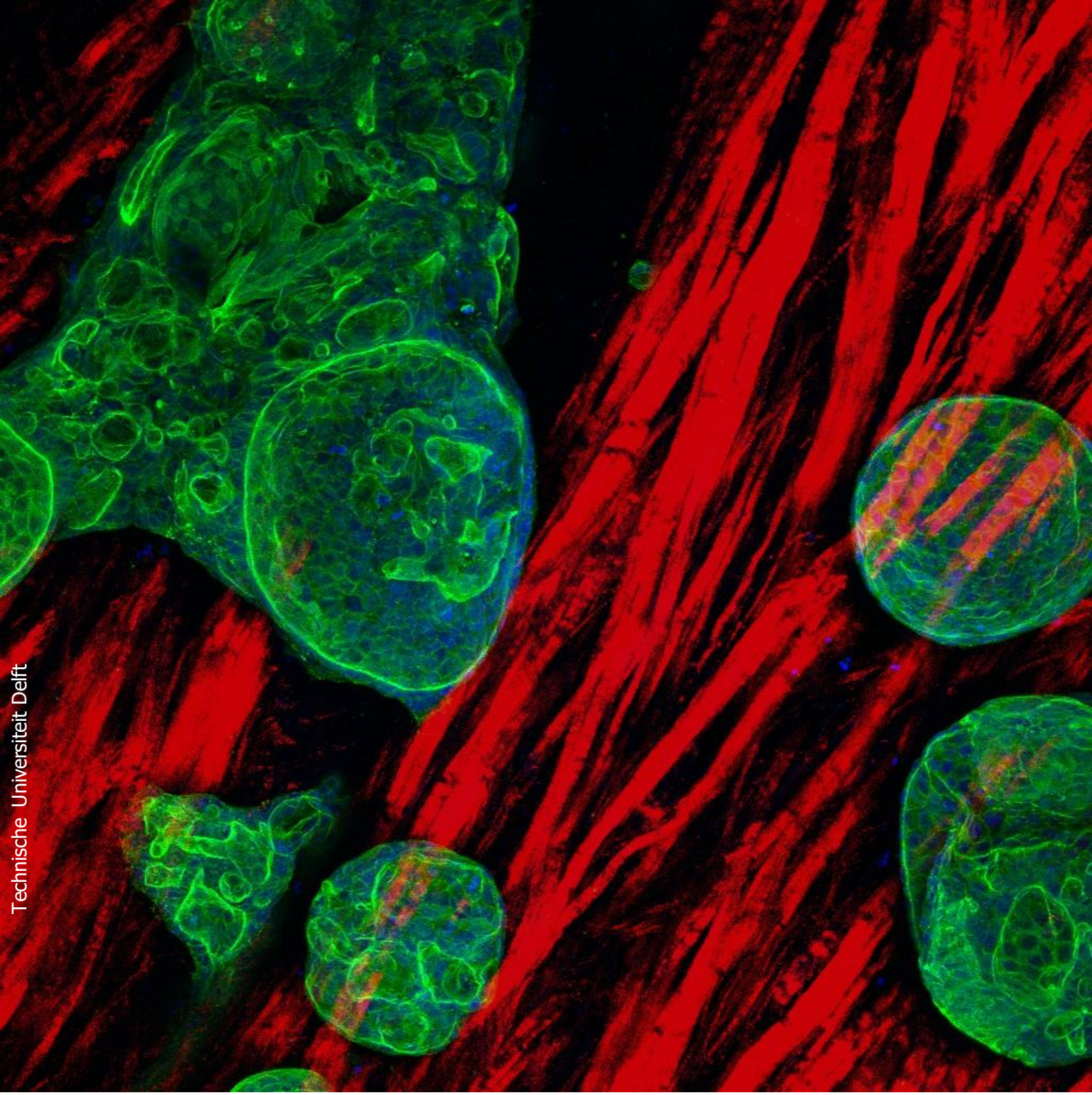

Technische Universiteit Delft

Modeling Primary Liver Cancer using Tumor-Derived Extracellular Matrix

Floor de Weijer

TU Delft

Erasmus MC
Universitair Medisch Centrum Rotterdam

Modeling Primary Liver Cancer using Tumor-Derived Extracellular Matrix

by

Floor de Weijer

to obtain the degree of Master of Science
at the Delft University of Technology,

Student number:	4757440	
Project duration:	February 1, 2019 – November 1, 2019	
Thesis supervisors:	Dr. M.M.A. Verstegen,	Erasmus MC
	Prof. dr. L.J.W. van der Laan,	Erasmus MC
	Dr. Ir. E. L. Fratila-Apachitei,	TU Delft
	Prof. dr. A. A. Zadpoor,	TU Delft, chair of the exam committee

TU Delft

Abstract

Due to the global health impact of primary liver cancer, resourceful models are required to develop new therapies and to study chemo-resistance. Recent advantages in understanding cancer complexity have shifted research to the importance of the niche of the tumor cells. In cholangiocarcinoma (CCA), an aggressive malignancy of the liver, the extracellular matrix (ECM) surrounding the cancer cells plays an essential role in tumor progression and chemo-resistance. To research potential mechanisms involved in drug-resistance it is necessary to grow CCA-derived cells in the vicinity of their native tumor micro-environment. Cell-free scaffolds can be created by decellularizing liver tissue contributing to the availability of new tissue engineering culture platforms. The resulting extracellular matrix can serve as a scaffold resembling the native non-cellular component of the tumor environment. However, a protocol to decellularize CCA tumor tissue is not yet established. It is not possible to use the traditional perfusion-based decellularization protocol for tumors, due to the lack of an intact capsule and vascular system to cannulate. The aim of this study is to develop a tumor scaffold retaining the essential characteristics of the extracellular matrix and to investigate its feasibility to serve as a scaffold for CCA-derived organoids.

To do this, CCA tumors were decellularized using an adapted protocol. Efficiency of removal of cells was determined by histology and analysis of DNA content and the preservation of collagen and tissue stiffness was assessed. Architecture of decellularized tumor was compared to architecture of decellularized normal liver tissue. A-cellular scaffolds were repopulated with CCA-derived organoids and ingrowth and viability of cells were evaluated by histology and confocal imaging. Metabolic activity and gene expression levels were compared to cells grown in standard basement membrane matrix (BME) gel and grown in normal liver a-cellular scaffolds.

After completing the protocol, tumor tissues were white in color and histological examination revealed no cells could be detected indicating complete decellularization. DNA content was slightly above the critical threshold indicating not all nuclear debris was removed. Characterization of the tumor tissue and normal liver matrices revealed markedly higher collagen content and higher stiffness in tumor tissue underlining the importance to differentiate between tumor and normal scaffolds. Recellularization of the scaffolds revealed that cells did not only attach to the surface, but also grow inside the scaffold. Comparable metabolic activity was observed between cells grown in tumor scaffold and in BME. We observed that cells seeded in tumor scaffolds showed different gene expression levels than those seeded in standard BME culture.

The resulting combination of CCA-derived organoids and tumor ECM provides an innovative basis for a model in which cell-extracellular matrix interactions can be studied. To make a complete culture platform, future studies should focus on including the cellular component of the tumor micro-environment. This will enable the identification of patient-specific drug sensitivity and to study mechanisms involved in drug-resistance.

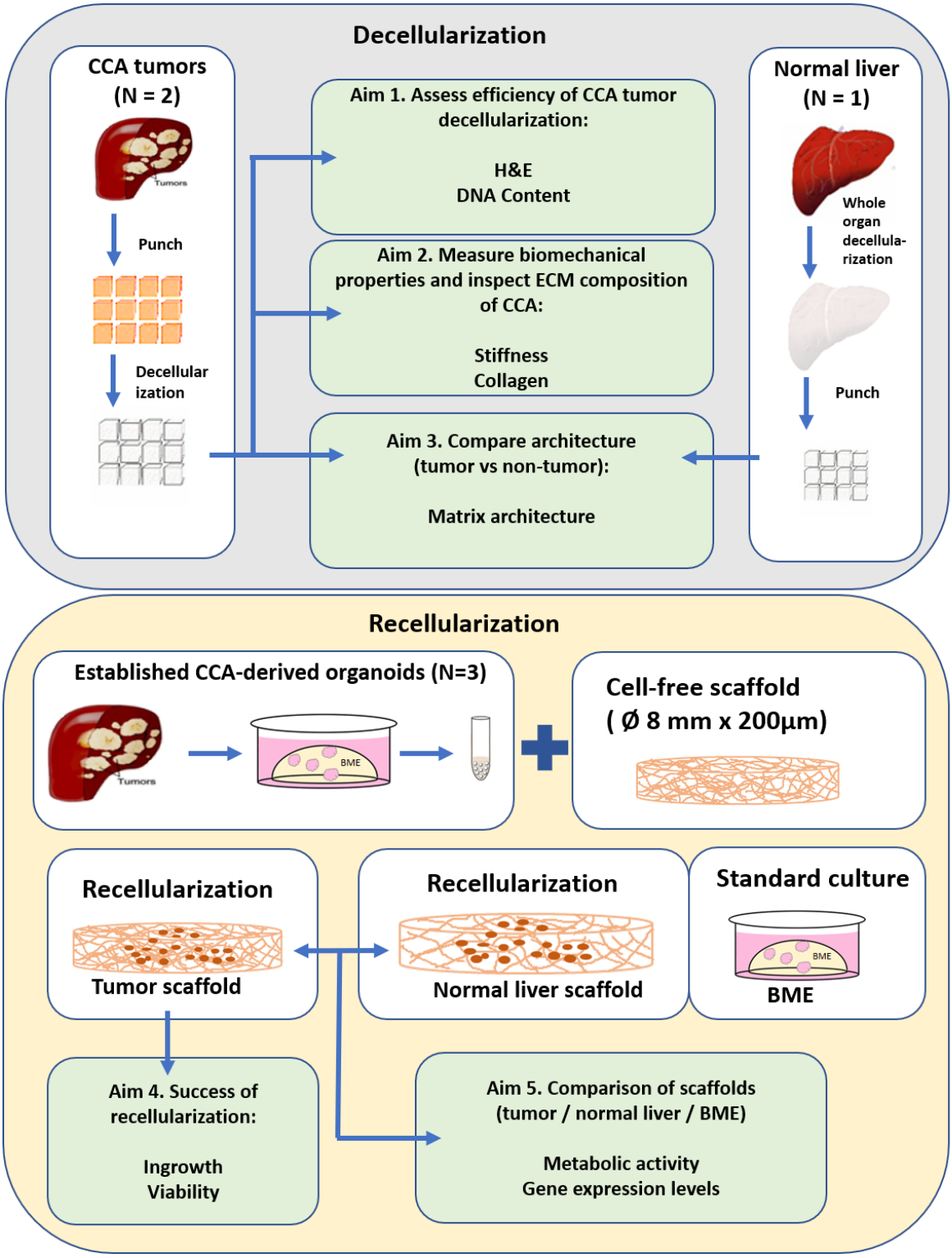

Figure 1: Graphical abstract of the study.

Contents

1 Introduction

1.1. Cholangiocarcinoma

Primary liver cancer is the second most common cause of cancer related death in men worldwide with a global mortality burden of 9% [1]. The two most common types of primary liver cancer are hepatocellular carcinoma (HCC) and cholangiocarcinoma (CCA). HCC develops from liver parenchymal cells (hepatocytes) whereas CCA is a bile duct cancer that develops from biliary epithelial cells (cholangiocytes). CCA is a rare disease but has a great clinical impact since the overall survival rates are low and it is responsible for 10-20 percent of deaths in primary liver cancer [2, 3]. Currently, the only curative treatment is surgical resection [4, 5]. However, late diagnoses of CCA in patients results in detection of CCA in an advanced disease stage making a high number of patients excluded from surgery [6]. The high mortality burden of CCA provokes research into finding new treatments. To date, chemotherapeutic interventions have been disappointing mostly due to patient-specific drug resistance [4, 7]. Therefore, there is need for an *in vitro* CCA model that closely mimics the native tumor to study mechanisms involved in drug-resistance and enable to uncover patient specific drug sensitivity.

1.2. Cell source for tumor engineering

Conservative methods to test anti-cancer treatments are two-dimensional (2D) cell culture models or animal models, both lacking the exact physiology of human liver cancer. Much research is done with the hepatocellular carcinoma cell line (HepG2) which are epithelial cells that can be cultured in 2D on plastic. These immortalized cell lines are easy to extent and are therefore a widely used cell source. However, they are not CCA specific. Established cell lines derived from cholangiocarcinoma are rare [8, 9]. With the intention to enable patient-specific drug testing, cell lines are not sufficient since autologous cells are required for personalized application. Moreover, 2D cell cultures lack the three-dimensional (3D) arrangement of cells and the interaction with their original tumor microenvironment. Therefore, other cell sources should be considered for CCA tumor engineering. A novel method to culture liver tumor cells allows primary tissues to grow in three-dimensional (3D) conditions. The cells self-organize into so-called organoids [10]. Organoids derived from CCA were recently established [11]. These cell cultures more closely mimic the original tissue function and architecture than cell lines [11, 12]. Moreover, the organoids resemble the intrinsic properties of the cancer cells important in drug-resistance and already led to the development of a potential therapeutic agent, ERK inhibitor SCH772984, for primary liver cancer [11]. Because of their extensive proliferative capacity, the CCA-derived organoids are capable to be expanded for long-term and are genetic stable during expansion [11]. Furthermore, organoids can successfully be established from resected tissue but also from core needle biopsies making them applicable in personalized medicine

[13]. However, these tumor organoids are currently grown in Basement Membrane Matrix (BME) or Matrigel Matrix, extracellular matrix hydrogels derived from mouse sarcoma cells. Hence these gels do not recapitulate the interaction of cell with the original extracellular matrix (ECM). Cancer drug resistance is dependent on both the intrinsic cancer cell properties as well as on their interaction with their environment. Consequently, the CCA-derived organoids might only partially recapitulate the original tumor. However, the genetic stability and the high expansion rate of organoids makes them a suitable cell source for tumor engineering.

1.3. Role of extracellular matrix in drug-resistance

The interaction of cancer cells and its dynamic environment is receiving growing interest as it may contribute to cancer development [11, 14–16]. The surrounding environment of the tumor cells is known as the tumor micro-environment and consists of a non-cellular component, the extracellular matrix, and a cellular component such as blood vessels, immune cells and fibroblasts. CCA is characterized for its aberrant hypersecretion of ECM components [17]. In epithelial cancers tumor stiffness and ECM composition is known to involve drug-resistance and tumor progression [4, 18]. The hard excessive matrix deposition constraints the delivery of chemotherapeutic reagents into the tumor [4, 17, 19]. Furthermore, intracellular mechanosensors respond to external mechanical forces conveyed by the stiffness of the matrix [20]. As a result, stiffening of the ECM may aggravate the proliferating and invading capacity of the cancer cells [21]. Recently developed therapies are aimed to reduce the stiffness of the desmoplastic stroma [21, 22]. Including the native ECM in the *in vitro* CCA cultures is necessary in order to study chemo-resistance in combination with ECM-targeting drugs. To date, there are no three-dimensional CCA culture models including ECM with correct mechanical and biochemical properties. Better understanding of the role of ECM in CCA development and progression may provide the basis to target ECM as a therapy.

1.4. Decellularization to obtain native extracellular matrix

The decellularization of tissue to obtain native extracellular matrix enables to create a scaffold with correct ECM composition and mechanical properties [23, 24]. However, this is not yet done with CCA-derived tumor tissue. The conventional way to obtain liver matrix is by controlled decellularization perfusion of a whole liver with detergents to remove all cells. In small rodents this is relatively easy, however upscaling to large livers, for instance from humans, is more challenging [25, 26]. Decellularization of whole human livers is optimized in our laboratory *(Verstegen et al., 2017)* and the scaffolds are currently used in liver tissue engineering projects [24]. Normal liver tissue may not represent the ideal ECM for tumor engineering. To gain pure tumor scaffold, tumors need to be isolated from non-tumorous adjacent liver tissue. It is obviously not possible to use perfusion-based decellularization of a tumor due to the lack of blood vessels to cannulate. Whole human livers containing a tumor are rarely available with intact capsule and vascular system which are necessary for decellularization using perfusion. Furthermore, tumors are notoriously known to have a necrotic core and are sometimes encapsulated, making it even more difficult to remove all cells and cellular debris within a tumor. Therefore, we needed to invent a method to remove all cells as we depend on small biopsies taken from primary liver tumors without damaging its ECM. Recently, a method to decellularize small tissues is developed resulting in an a-cellular tissue where the ECM-proteins, 3D-architecture, topography and mechanical properties are maintained [23]. In this project, this method was customized to decellularize human liver tumor biopsies to create a scaffold for tissue engineering.

1.5. A-cellular scaffold

Decellularized tissue can be used as a 3D scaffold for cells. HepG2 cells have already been successfully grown in non-tumor liver a-cellular scaffolds and exhibit markedly different gene expression when compared to the standard 2D cell culture [23]. The resulting *in vitro* model is bioengineered liver tissue where the cells engraft, are viable and express a functional phenotype up to 14 days. However, this is not yet done with CCA tumor tissue which has a more dense ECM. In this project we have focused on creating a scaffold including the native ECM by decellularization and to repopulate it with CCA derived organoids. Specifically, the hypothesis is tested that non-tumor and tumor ECM differently effect cell behavior in terms of gene expression and metabolic activity.

1.6. Aim of the project

The main aim of this study is to develop a tumor scaffold retaining the essential characteristics of the non-cellular component of the tumor micro-environment and to investigate its feasibility to serve as a scaffold for CCA-derived organoids.

To create a cell-free scaffold containing the tumor extracellular matrix the first step was to decellularize CCA tumor tissue and to assess the efficiency of the removal of cells. Since the decellularization process can cause alterations in the composition and biomechanical properties of the matrix the next goal was to inspect the collagen composition and to measure the stiffness of the tumor tissue before and after decellularization. Epithelial tumors are known for their aberrant deposition of ECM. Subsequently, the following step was to compare the architecture of the tumor matrix with the matrix of normal liver tissue obtained via whole-organ perfusion.
Concerning the repopulation of the scaffolds, the next step was to repopulate the obtained a-cellular scaffold with CCA-derived organoids and to assess the growth and viability of the cells into the scaffold. The interaction that the cells establish with the extracellular matrix can largely determine the behavior of the tumor. Therefore, the last goal was to compare cell behavior of cells grown in tumor scaffolds, normal liver scaffolds and the standard BME culture in terms of metabolic activity and gene expression levels.

2

Methods

2.1. Decellularization

2.1.1. Source of tumors

Tumor samples (n=2, ±30 cm^3) were obtained during a partial resection procedure to remove the tumor from two patients with CCA. Use of both tissues for research purposes was approved by the Medical Ethical Council of the Erasmus MC and informed consent was given (MEC-2014-060). Both tumors were derived from moderately differentiated CCA. Each sample was split into three parts: one big part saved to be decellularized, one part processed for histology and DNA content analysis, and one part intended for nanoindentation.

2.1.2. Tumor decellularization

The samples destined for decellularization were frozen at -20 °C for a minimum of 24 hours. This enabled the first destruction of cell membranes in the tissue as intra-cellular ice crystals disrupt the cell membrane. While still frozen, small and uniform tissue samples were made using a disposable biopsy punch to create an 8 mm diameter cylinder. Tissue biopsies were again frozen at -20 °C until further use. Tissues were thawed and washed in 50 ml phosphate buffered saline 1X (PBS, Gibco) in a 50 ml tube at room temperature for 1 hour. Removal of cells and cell debris was performed by submerging the tissue cylinders in 50 ml 4% Triton X-100 (Brunschwig Chemie, Amsterdam, Netherlands) supplemented with 1% ammonium hydroxide at 37 °C at 200 revolutions per minute (rpm) overnight (O/N). Solution was changed to dH_2O for one hour. These steps were repeated for 3 times as described in Table 2.1. Hereafter, to breakdown and remove remnants of DNA fragments sticking to the matrix the tissue was submerged in a DNAse-I solution (2 mg/L; Roche, Mannheim, Germany) at 37 °C at 200 rpm for 3 hours, followed by washing the cylinder 3 times in 50 ml 1% PBS. Each cylinder was split into three parts: one big part saved to be prepared as a scaffold, one part processed for histology and DNA content analysis, and one part intended for nanoindentation.

Table 2.1: Protocol for decellularization of small tumor biopsies. Used abbreviations: deionized water (dH_2O), phosphate buffered saline (PBS), overnight (O/N).

Step	Solution	Temperature (°C)	Time (hours)	Volume (ml)	Repetitions
1	dH_2O	RT	1	50	1
2	4% Triton X-100 + 1% Ammonia	37	O/N	50	Repeat Step 2 - 5 3x
3	Hypertonic saline	37	1	50	
4	dH_2O	37	1	50	
5	PBS	37	1	50	
6	DNAse	37	3	50	1
7	PBS	37	1	50	3x

2.1.3. Whole organ decellularization

As comparison, previously decellularized non-tumor donor liver tissue was included in this study (n=1). For this, a whole liver, discarded for transplantation due to bad quality, was decellularized using machine perfusion using the same detergents. Decellularization was performed as described by a manuscript submitted for publication, Willemse et al., 2019 [27]. While the decellularized liver was frozen, small and uniform biopsies were made using a disposable biopsy punch to create an 8 mm diameter cylinder.

2.2. Recellularization

2.2.1. Organoid cell culture

Organoids initiated from tumors of three CCA patients (n=3) were already established and characterized according to a previously described protocol [11]. Organoids were derived from moderate to moderate/well differentiated CCA tumors. Notice that these tumors are derived from different patients than the tumors destined for decellularization and tissue characterization. Passaging of the organoids was done by mechanical dissociation into small fragments with a 200 µl pipet tip and transferred to fresh Basement Membrane Extract (BME, Type 2, Pathclear) with a consistent ratio of 1:6-1:8 every 7 days or upon attainment of a dense culture. Expansion medium was changed twice a week. The components of the expansion medium are listed in Supplemental Table S1.

2.2.2. Scaffold preparation for recellularization

The decellularized scaffolds were prepared for recellularization by embedding the decellularized samples in optical cutting temperature (OCT) compound, mounting it on a metal holder, and cutting 200 µm thick frozen slices with a cryostat at -13 °C. Scaffolds were collected in a 50 ml tube and frozen until further use. One day before cell seeding, scaffolds were thawed at room temperature in 50 ml sterile PBS. OCT compound was removed by washing 3 times with sterile PBS supplemented with 1% penicillin streptomycin (PS) at room temperature. Followed by incubation in Advanced DMEM/F12 supplemented with 1% PS overnight. Before seeding, the scaffolds were washed again two times with advanced DMEM/F12 supplemented with 1% PS followed by washing three times with Advanced DMEM/F12 supplemented with 50 µg/ml Primocin, 1% Ultraglutamine and 10 mM HEPES. Subsequently, each scaffold slice was placed in a well of a 48 well plate and surrounding medium was removed.

2.2.3. Recellularization of a-cellular scaffolds

The CCA tumor-derived organoids grown in BME were washed in cold advanced DMEM/F12 supplemented with 50 µg/ml Primocin, 1% Ultraglutamine and 10 mM HEPES to remove BME and centrifuged at 1500 rpm for 5 minutes at 5 °C. The supernatant was removed and 1 ml of trypsin was

added for 10 minutes on 37 °C to gain a single cell solution. Advanced medium was added to stop trypsin activity and cells were counted manually using a Burker-Turk cell counting chamber. The cells were spinned down at 1500 rpm for 5 minutes at 5 °C. The resulting cell pellet was resuspended in Expansion Medium supplemented with 10 µM Y276322 in a concentration of 100000 cells per 10 µl. The 10 µl cell suspension was released on the a-cellular scaffold slices in the 48 well plate by dropping it on the scaffold. As a control, 25000 tumor organoid cells were resuspended in 6.25 µl expansion medium supplemented with 10 µM Y276322 and 18.75 µl cold BME and plated in a 48 well plate according to standard organoid culture procedures [11, 12]. After cell seeding in scaffolds or BME, the plates were kept at 37 °C during 4 hours in a humidified incubator containing 5% CO_2 to allow cell attachment to the scaffold. After this, 300 µl of expansion medium supplemented with 10 µM Y276322 was added to the wells, to ensure colony formation of the organoids. Expansion medium was refreshed every 2-3 days. Only during the first three days Y276322 was added to the expansion medium. Recellularized scaffolds were assessed using brightfield microscopy on EVOS cell imaging systems at day 1, day 8 and day 14. At 14 days of incubation, the scaffolds were collected for histological examination, confocal imaging, LIVE/DEAD assessment or mRNA expression analysis.

2.3. Analysis

2.3.1. DNA quantification

After the first freezing step (t = non-decel) and after decellularization (t = decel), a small piece (± 10 mg) of the tissue was isolated for DNA quantification and kept at −80 °C until further analysis. Tissues were weighted and if necessary, cut to be maximal 10 mg in mass. 20 µL proteinase K solution (Qiagen) was added to each sample and placed at 56 °C on a rocker at 80 rpm overnight until completely lysed. QIAamp DNA micro kit (Qiagen) was used to isolate DNA according to the manufacturer's protocol. Extracted DNA was diluted in 50 µl of dH_2O and quantified using the NanoDrop spectrophotometer (Thermo Scientific, Breda Netherlands). Data was analyzed by Student's t-test using GraphPad Prism version 8.00.

2.3.2. Histology

Fresh tissue and decellularized tumor tissue were fixed for 24 hours at 5 °C in 4% formalin and washed with PBS. Fresh and decellularized tissue was embedded in paraffin according to standard procedure. Recellularized scaffolds were collected after 14 days. Reseeded scaffolds were fixed for 30 minutes at room temperature in 4% formalin and embedded in agarose followed by paraffin embedding. After paraffin embedding tissues were cut with 5 µm section thickness using a microtome and collected on a glass microscope slide. To analyze the efficiency of decellularization or recellularization the sections were stained with haematoxylin and eosin (H&E) to stain nuclei and cytoplasm, respectively. Deparaffinization of glass slides was done by two changes of xylene and incubation in decreasing concentrations of ETOH (100, 90, and 70%) for 5 minutes. Slides were incubated in freshly filtered haematoxylin (Mayer's Hemalum solution) for 2 minutes, dipped in acid ethanol and rinsed in tap water. Sections were stained with eosin (0.5%) for 30 seconds and washed again with running tap water. Sections were dehydrated by incubating them for 5 minutes in increasing concentrations of ETOH (70, 90, and 100%), placed in two changes of xylene for 5 minutes and mounted with Pertex. To analyze collagen content, sections were deparaffinated and incubated with Picrosirius Red (PSR)(F3B - C.I. 35782) for 60 minutes followed by two dips in acidic water followed by dehydration series, placed in xylene and mounted with Pertex. All stained sections were analyzed using a Zeiss Axioskop 20 microscope and captured with a Nikon DS-U1 camera. To stain nuclei, paraffin sections were dehydrated and stained with 4',6-diamidino-2-phenylindool (VECTASHIELD® Antifade Mounting Medium with DAPI) and analyzed by fluorescence microscopy on EVOS cell imaging systems with the same light gathering power for all conditions.

2.3.3. Nanoindentation

The stiffness of the CCA tissue before and after decellularization were assessed with nanoindentation measurements with the PIUMA Nanoindenter (Optics11, Amsterdam) using a spherical cantilever with tip radius 50 µm and stiffness 0.50Nm. For this, tissue slices (approximately 2 mm height) were cut and kept in PBS at 5 °C until further analysis. The slices were attached to a petri dish using cyanoacrylate adhesive on the whole bottom surface. After attachment, the slices were immersed in PBS. Each sample was measured at 3 locations. At every location a matrix consisting of 3 X-locations and 3 Y-locations was measured with a distance of 100 µm apart to avoid overlap considering the Hertz contact model [28]. A slow indentation speed of 2.5 µm/s was used to overcome the viscoelastic behavior of the tissue. The total indentation depth was 10 µm. Each indentation was measured in triplo. Measurement where no contact point could be determined were discarded resulting in a total of 67 force-distance curves for fresh CCA tissue and 81 force-distance curves for decellularized CCA tissue. Elastic moduli were calculated from the force-distance curves by the Hertzian contact model using the Piuma Dataviewer Software. Non-tumor tissue was not measured since the fresh non-tumor tissue was not preserved upon the beginning of this study. Comparison between two groups were made by Mann-Whitney U Test using GraphPad Prism version 8.00.

2.3.4. Cell viability

For LIVE/DEAD assessment, recellularized scaffolds were transferred to a small petri dish and incubated in expansion medium containing 100 µg/ml Hoechst 33342 , 12.5 µg/ml propidium iodide (PI, Sigma-Aldrich), 1 µM calcein acetoxymethyl ester (Calcein AM, Thermo Scientific) for 30 minutes at 37 °C in dark and imaged leaving the dye on. Hoechst is a fluorescent dye binding to all DNA (blue). PI is a fluorescent dye that binds to DNA in dead cells (red). Calcein AM is fluorescent upon entering only viable cells (green). Images were captured with an EVOS fluorescent microscope or with the Leica SP5 inverted confocal microscope.

2.3.5. Confocal imaging and SHG multiphoton analysis

Formalin-fixed sections were whole mount stained with Alexa Fluor 488 Phalloidin and DAPI mount. Sections were transferred to a petri dish and covered in PBS. Images were obtained with a Leica SP5 AOBS with multiphoton laser. The APO dipping lens (20x) with numerical aperture of 1.00 was used to deliver the excitation signal and to collect the emission signal. The autofluorescence of collagen 1 was collected using 880 nm excitation. Averaging was performed over 4 lines for Second Harmonic Generation (SHG) to reduce the effect of noise. DAPI signal was collected using 496 nm excitation and 458 nm emission. Alexa Fluor 488 signal was collected using 448 nm excitation and 514 nm emission. Images were obtained with a 1024 pixel resolution and a 5 µm or 2.5 µm z-step size. The images were processed using ImageJ to obtain Maximum Intensity Projection (MIP) images.

2.3.6. Metabolic activity

To assess metabolic activity, Presto Blue Cell Viability Reagent (ThermoFisher) was performed on day 1, 3, 7 and 11. Day 1 was measured 24 hours after seeding. The Presto Blue assay was diluted 1:10 in expansion medium and put in the wells after carefully removing the expansion medium. The scaffolds were incubated in dark at 37 °C, 5% CO_2 for 4 hours. After incubation the medium was plated in triplicate in a 96 wells plate. The absorbance was recorded with excitation of 530 nm and emission of 590 nm using an Omega POLARstar Microplate reader (BMG labtech). Five biological replicates were performed for each of the three CCA-derived organoid lines. Empty scaffolds without cells were taken along to distract background absorbance. Background was subtracted and data was normalized to day 1 to compensate for differences in cell numbers seeded. Data are expressed as mean ± SD and analyzed by repeated measures ANOVA using GraphPad Prism version 8.00.

2.3.7. RNA extraction and RT-PCR

Fourteen days after recellularization, five biological replicates were collected for each scaffold (n=3) seeded with each patient-derived cell culture (n=3). RNA was extracted from scaffolds using Qiazol Lysis reagent and RNeasy mini kit (Qiagen) following manufacturer's instructions and quantified using the NanoDrop spectrophotometer (Thermo Scientific, Breda, Netherlands). 500 ng of total RNA was reverse transcribed to synthesize cDNA. cDNA was amplified with iTaq Universal SYBR Green Supermix and using gene-specific primers described in Supplemental Table S2. Gene expression was measured with the Applied Biosystems 7500 Real-Time PCR system. The delta CT method was used to calculate gene expression levels and normalized to the housekeeping genes. Housekeeping genes were GAPDH and B2M which were geometrical averaged [29]. Each of the three CCA-derived organoid lines were grown in non-tumor scaffold, two CCA scaffolds and in BME. Data was analyzed by One-way ANOVA using GraphPad Prism version 8.00.

3

Results

3.1. Decellularization

3.1.1. Decellularization of human CCA-derived tumor tissue

CCA-derived tumor tissue was decellularized with the purpose to generate an a-cellular scaffold including native tumor extracellular matrix. As illustrated by Figure 3.1 A and B the tumor tissue appeared macroscopically white and transparent following the 4 day decellularization protocol. Paraffin sections stained with haematoxylin and eosin staining revealed that no cell debris and nuclei were detected within the tissue after decellularization while the ECM architecture remained intact (Figure 3.1 C and D). The removal of cells was further confirmed by DAPI staining which showed no cellular nuclei were detected after decellularization providing evidence for complete decellularization of the tumor tissue (Figure 3.1 E and F).

The DNA amount was quantified after the first freeze-thaw cycle (non-decellularized) and after decellularization in order to determine efficiency of genetic material removal. DNA content was significantly reduced by 88% (p-value = 0.006, Figure 3.2 A). The absolute DNA content of decellularized tissue was 62.3 ng/mg (Figure 3.2 B).

3.1.2. Decellularization of normal liver tissue

The decellularization protocol to decellularize small biopsies did not effectively remove fat. Normal tissue appeared macroscopically yellow/brownish after decellularization (Supplemental Figure S1 A). Fat reduced after treatment with isopropanol (Supplemental Figure S1 B and C). However, isopropanol is known to damage the ECM components. To ensure the preservation of ECM ultrastructure and proteins and guarantee the absence of fat, it was chosen to use decellularized non-tumor tissue obtained via whole liver decellularization perfusion. Previously performed work confirmed the removal of cells by H&E staining after decellularization where images are originating from a paper submitted for publishing (Willemse et al., 2019) [27])(Supplemental Figure S2).

3.1.3. Biomechanical properties of CCA tissue

As tissue stiffness is an important parameter of tumor initiation and progression, the biomechanical properties of the tissues were measured using a nanoindenter. The Young's Modulus calculated for the non-decellularized CCA tissue was 4.53 (kPa) and for the decellularized CCA tissue 2.93 (kPa). No significant differences in Young's Modulus were found upon decellularization (Figure 3.3 A). It must be noted that a high heterogeneity within the tissues is observed leading to a high standard deviation of the mean as visualized in Figure 3.3 B.

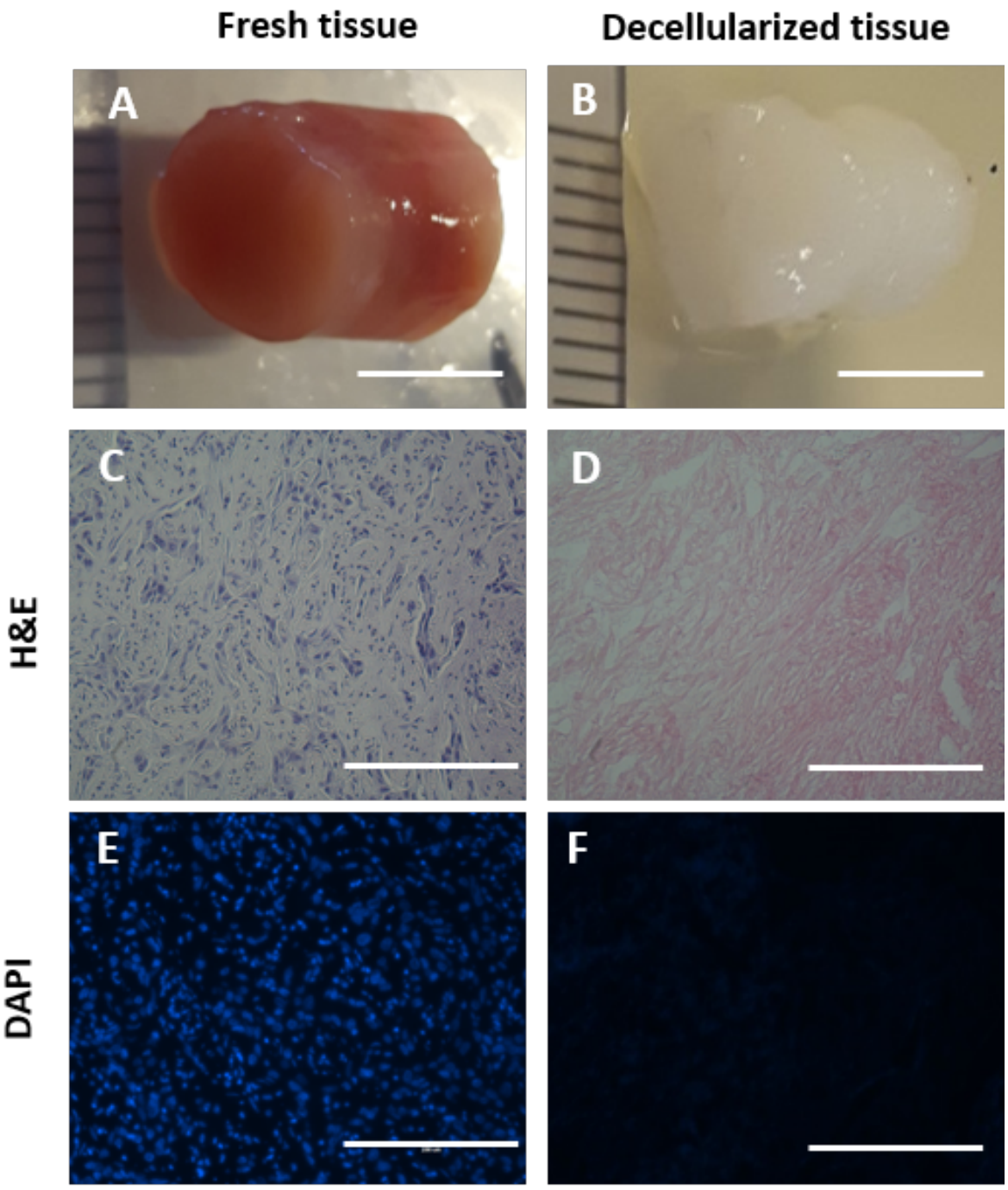

Figure 3.1: Effective removal of cells after decellularization of CCA-derived tumor tissue biopsies (ϕ 8 mm). **(A, C, E)** Fresh CCA-derived tumor tissue and **(B, D, F)** decellularized CCA-derived tumor tissue. **(A, B)** Macroscopic appearance of biopsies after decellularization indicated efficient removal of cells. Scale bars represent 0.5 cm. **(C, D)** Histological staining with H&E confirmed elimination of cellular material. Scale bars represent 100 µm. **(E, F)** Removal of nuclear material is confirmed by DAPI staining. Scale bars represent 200 µm. Representative images are chosen.

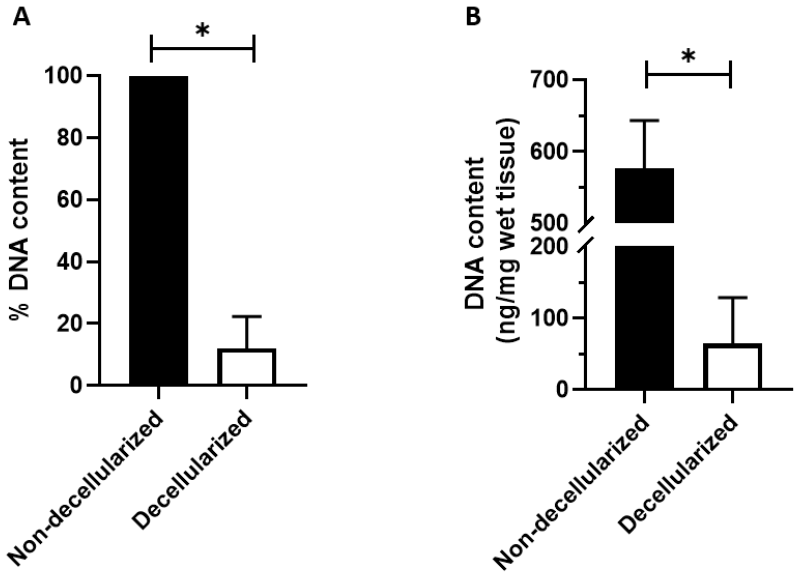

Figure 3.2: Quantitative DNA content before and after decellularizion of CCA-derived tumor tissue. **(A)** Non-decellularized tissue is measured after the first freeze-thaw cycle. After decellularization the DNA content of decellularized CCA tissue decreased significantly by 88% compared to DNA content detected in non-decellularized tissue. **(B)** Absolute DNA quantification expressed as nanogram per milligram wet weight tissue showing DNA content of decellularized CCA tissue was 64.3 ng/mg. Data are expressed as mean ±SD. Matrices of two different patients were analyzed (N=2) and two biological replicates were performed per patient. Student's t-test (*p<0.05).

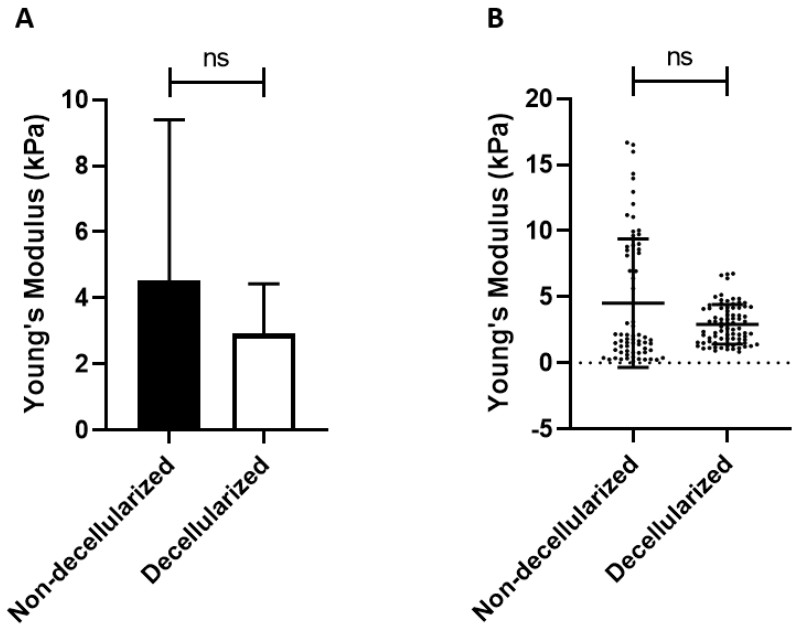

Figure 3.3: Young's Modulus of fresh and decellularized CCA tissue measured by nanoindentation. **(A)** No significant differences regarding stiffness were found between fresh and decellularized CCA tissue. **(B)** High heterogeneity of stiffness was found within the tissues. Each dot represents an individual indentation (fresh: 67 indentations; decellularized: 81 indentations). Data are expressed as mean ± SD. Mann-Whitney U test (ns indicated p> 0.05).

3.1.4. Comparison of collagen distribution between normal liver and CCA tissue

Next, the collagen content and tissue architecture were evaluated. Collagens were found to be present in similar density in the decellularized tissue in both tumor and non-tumor tissue compared to fresh conditions which confirmed the preservation of collagen type 1 and 3 upon decellularization (Figure 3.4). The collagen in the tumor ECM was disorganized and compact whereas in the non-tumor ECM the collagen fibers were less compact and it is possible to observe a more reticulated organization of the collagen fibers (Figure 3.4 C,D). Thus, the generated scaffolds conserve the native tissue differences between non-tumor tissue and CCA tumor tissue.

Altogether these results confirm the validity of the used decellularization protocol to obtain native tumor ECM intended for tumor engineering.

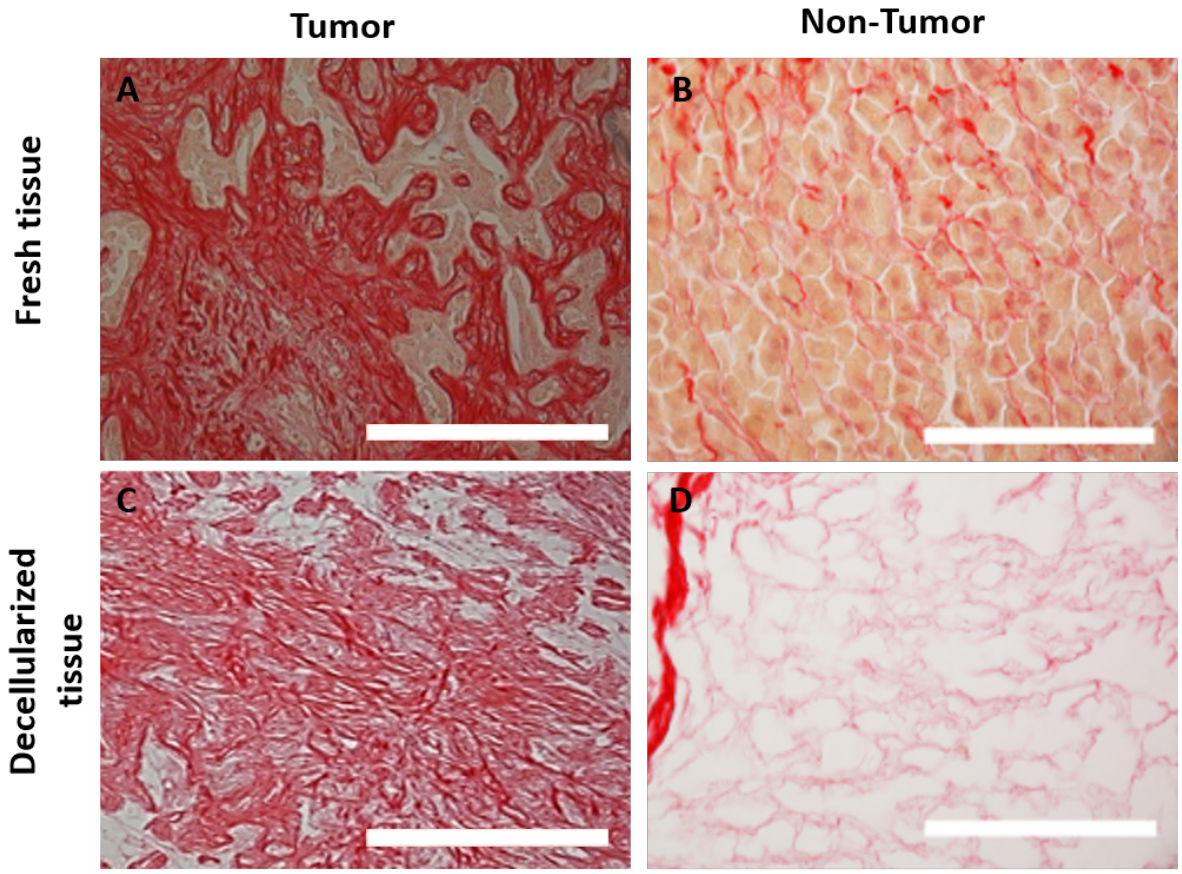

Figure 3.4: Preservation of collagen after decellularization of CCA-derived tumor and non-tumor tissue. **(A)** Fresh CCA tumor tissue and **(C)** decellularized CCA tumor tissue. **(B)** Fresh non-tumor tissue and **(D)** decellularized by perfusion non-tumor tissue. Picrosirius red staining of fresh and decellularized tissue confirmed the preservation of collagen type 1 and 3. ECM collagens were more organized in non-tumor tissue as compared to tumor tissue. Collagen was denser in CCA tissue compared non-tumor tissue. The generated scaffolds conserve the native tissue differences between non-tumor and CCA tumor after decellularization. Representative images. Scale bars represent 100 µm.

3.2. Recellularization

3.2.1. Recellularization of non-tumor and CCA tumor scaffolds

Next, it was investigated whether the decellularized tissues can serve as an a-cellular scaffold for CCA-derived organoids. For this, the decellularized non-tumor and CCA tumor cylinders were sectioned in 200 µm thick slices to create ECM scaffolds. The non-tumor and CCA tumor scaffolds were reseeded with CCA-derived cells by releasing the cells suspension on top of it. The first aim was to evaluate whether this technique led to the migration of cells into the scaffold. Within 1 day after cell seeding, the cells were found single cell and in small groups of cells in the scaffolds as imaged by brightfield microscopy (Figure 3.5). After 8 and 14 days the cells formed colonies. The colony forming of cells is comparable to the ones growing in the BME which serves as a control. Since it is hardly possible to determine depth using brightfield microscopy another technique was needed to determine whether the cells were found inside the scaffold. H&E staining of the cross sections of the engineered tissue revealed that cells attach to the outside of the scaffold (Figure 3.6 A) as well as were found inside the ECM scaffolds after 14 days (Figure 3.6 B and C). Likewise, the sections were collected in a sequence to visualize the cell distribution throughout the tumor scaffold in 3D (Figure 3.7). The sequence of two-dimensional cross-sections confirmed the occupation and migration of cells into the extracellular matrix at day 14.

3.2.2. Confocal imaging of recellularized scaffolds

To get a 3D image of the morphology of the cells attachment to the tumor scaffold and their distribution over the surface, confocal images were obtained after staining the actin filaments and nuclear material. Second Hormonic Generation was used to image collagen type 1. Maximum Intensity Projection images of the confocal images confirmed the growth of cells over the surface and following the contour of the tumor scaffold surface at day 14 (Figure 3.8). The cells were polygonal in shape with regular dimensions and were attached to the scaffold in discrete patches and appear epithelial like (Figure 3.9).

Altogether these imaging techniques illustrate that cells spread over the surface of the scaffold and engrafted into the scaffold.

3.2.3. Viability

To assess the survival of the cells, the viability of the CCA-derived organoid was analyzed using a LIVE/DEAD assay. Fluorescent imaging of the scaffolds revealed that cells were viable at day 14 (Figure 3.10). Dead cells in the middle of cell groups are observed indicating not all cells survived. A confocal maximum intensity projection image, which gives better resolution, revealed more live than dead cells on the edge of the repopulated scaffold (Figure 3.11).

3.2.4. Metabolic activity

To compare the effect of non-tumor and tumor scaffolds on the metabolic activity of CCA-derived cells a Presto Blue Assay was performed over 11 days of culture. This also enabled to monitor the metabolic activity of the engineered tissue over time. In the reseeded tumor and non-tumor scaffolds the CCA cells showed increasing metabolic activity during 11 days of culture (Figure 3.12). The elevation of metabolic increase was the highest between day 7 and day 11. At day 11 a significant difference was found between the metabolic activity of cells seeded in the CCA tumor scaffold compared with cells seeded in the non-tumor scaffold. Cells seeded in BME showed the same trend of metabolic activity increase. A significant higher metabolic activity of cells grown in BME has been detected compared to the non-tumor scaffold. No significant difference has been detected between BME and CCA scaffold. These findings demonstrate adequate metabolic function of cells grown in CCA scaffolds.

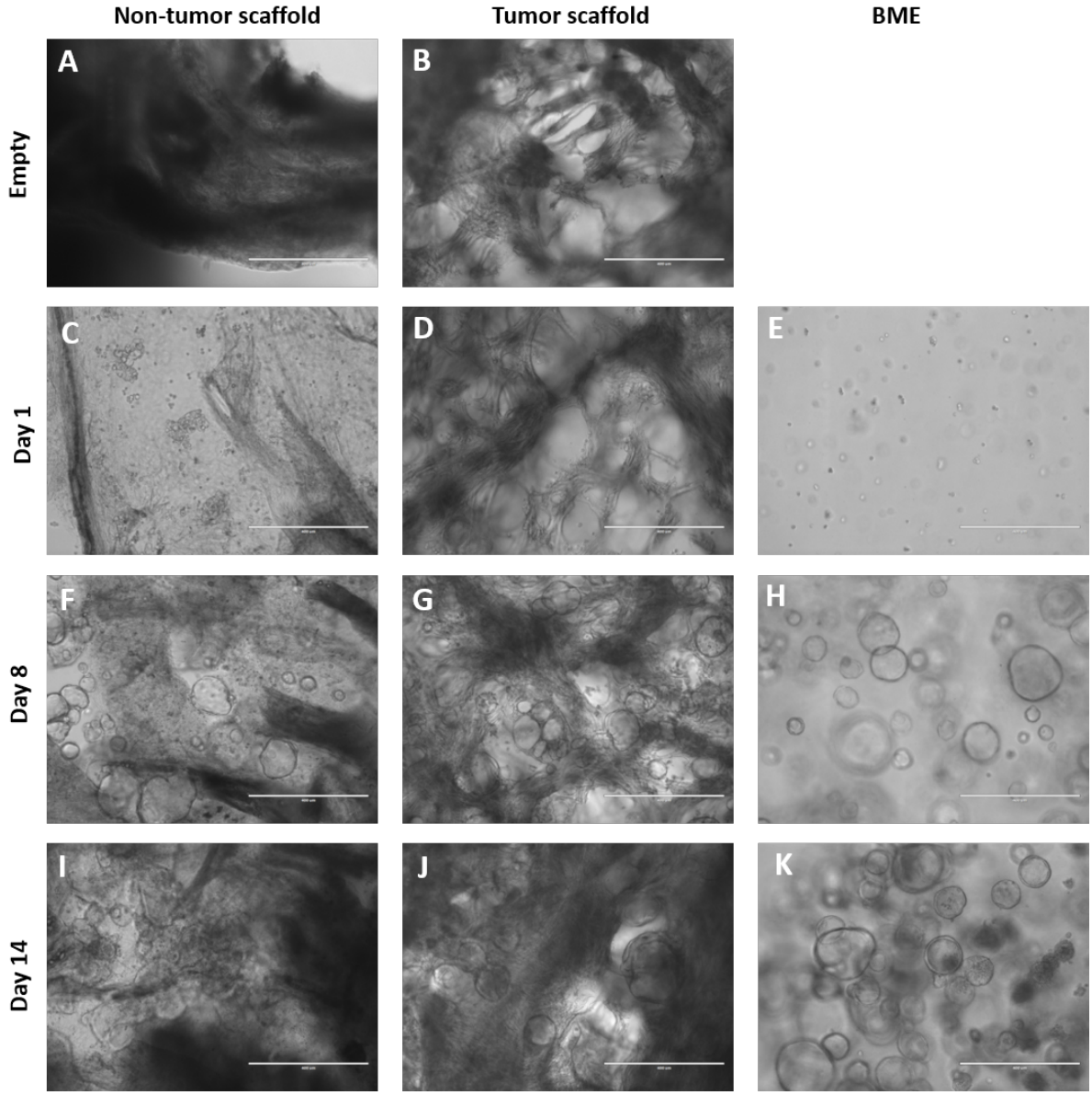

Figure 3.5: Representative light microscopy of CCA-derived organoids cultured in different 3D scaffolds. Cells grown in scaffolds derived from decellularized CCA **(A, C, F, I)** , non-tumor **(B, D, G, J)** and in standard BME hydrogel **(E, H, K)**. At day 1 in both ECM scaffold as BME control single cells were visible **(C, D, E)** whereas cell colony formation was observed at day 8 **(F, G, H)** and day 14 **(I, J, K)**. Representative images of CCA-derived organoid from one patient. Scale bars represent 400 µm.

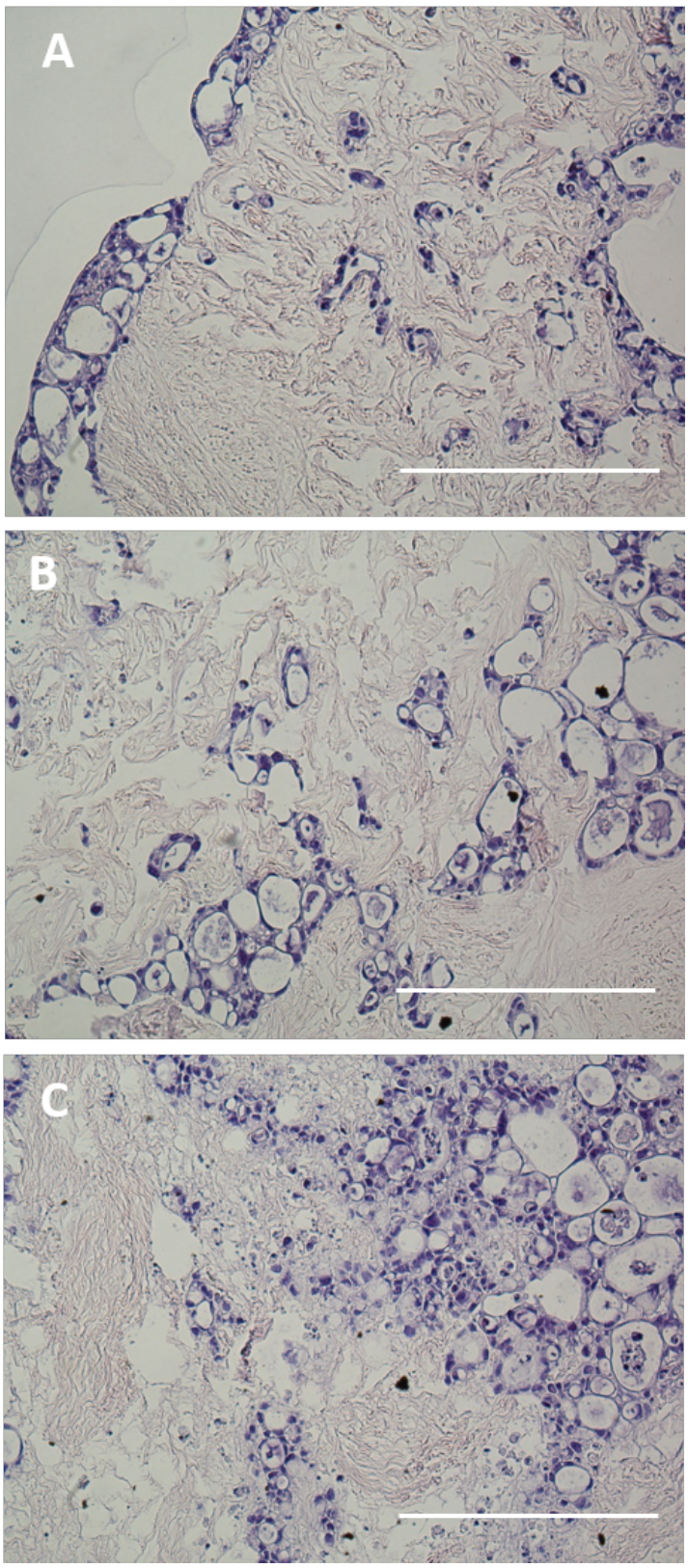

Figure 3.6: CCA-dervied cells grew inside the ECM scaffolds. Histological H&E staining of the tumor and non-tumor scaffolds reseeded with CCA-derived organoids from 1 patient after 14 days. **(A)** CCA-derived organoids attach to the outer surface of the scaffold and **(B)** are able to migrate into the scaffold. **(C)** Cells were found inside the non-tumor scaffold. Scale bars represent 200 µm.

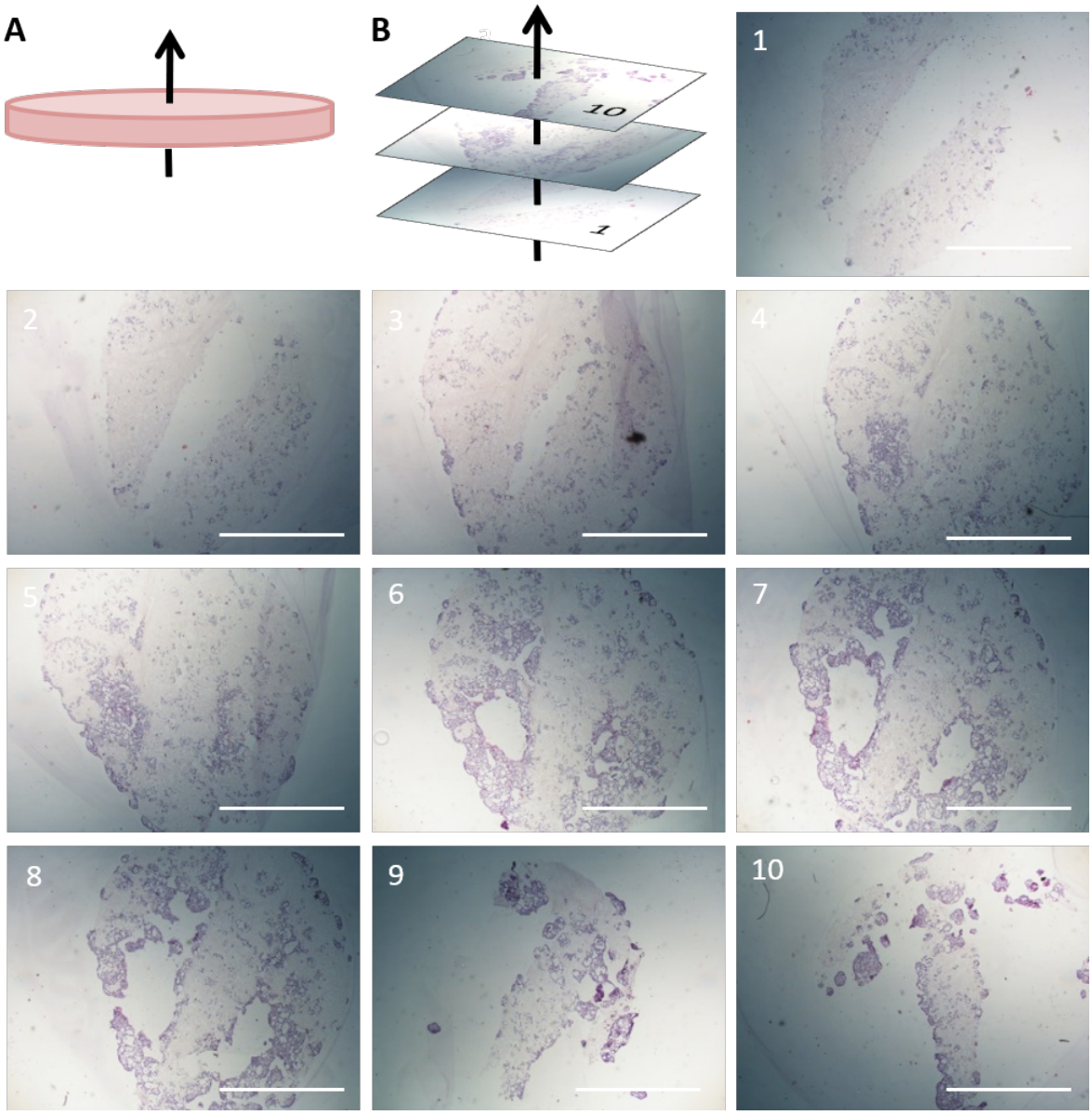

Figure 3.7: Multiple paraffin sections collected in a sequence revealing the ingrowth of CCA-derived organoids in the CCA tumor scaffold. **(A, B)** Images illustrating the direction of collection of the sections through the scaffold. **(1-10)** H&E staining of sections from the bottom (1) to the top of the scaffold (10) confirm the engraftment of cells throughout the scaffold. Scale bars represent 2000 µm.

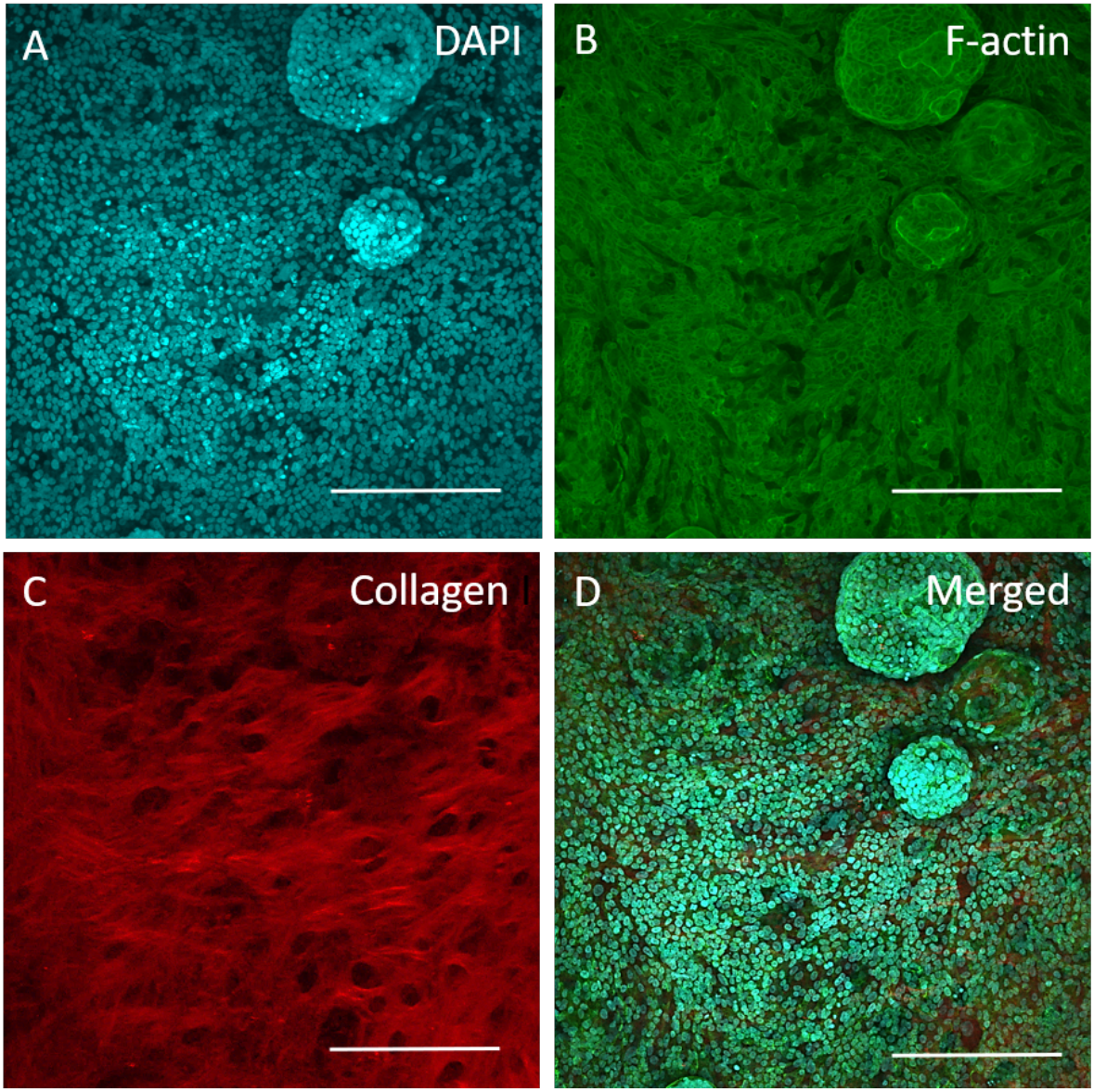

Figure 3.8: Representative confocal image of nuclei and actin staining and multiphoton image of collagen of CCA-derived organoids repopulating tumor decellularized matrix after 14 days. **(A, cyan)** Cell nuclei were labeled with DAPI, **(B, green)** actin filaments were labeled with Phalloidin. **(C, red)** Multiphoton microscopy images of repopulated scaffold. **(D)** All three channels are merged to show actin filaments, nuclei and collagen together. CCA-derived organoids covered the whole scaffold surface. Some leakage of DAPI signal is visible in the multiphoton channel since nuclei are visible in the channel. Scale bars represent 100 µm.

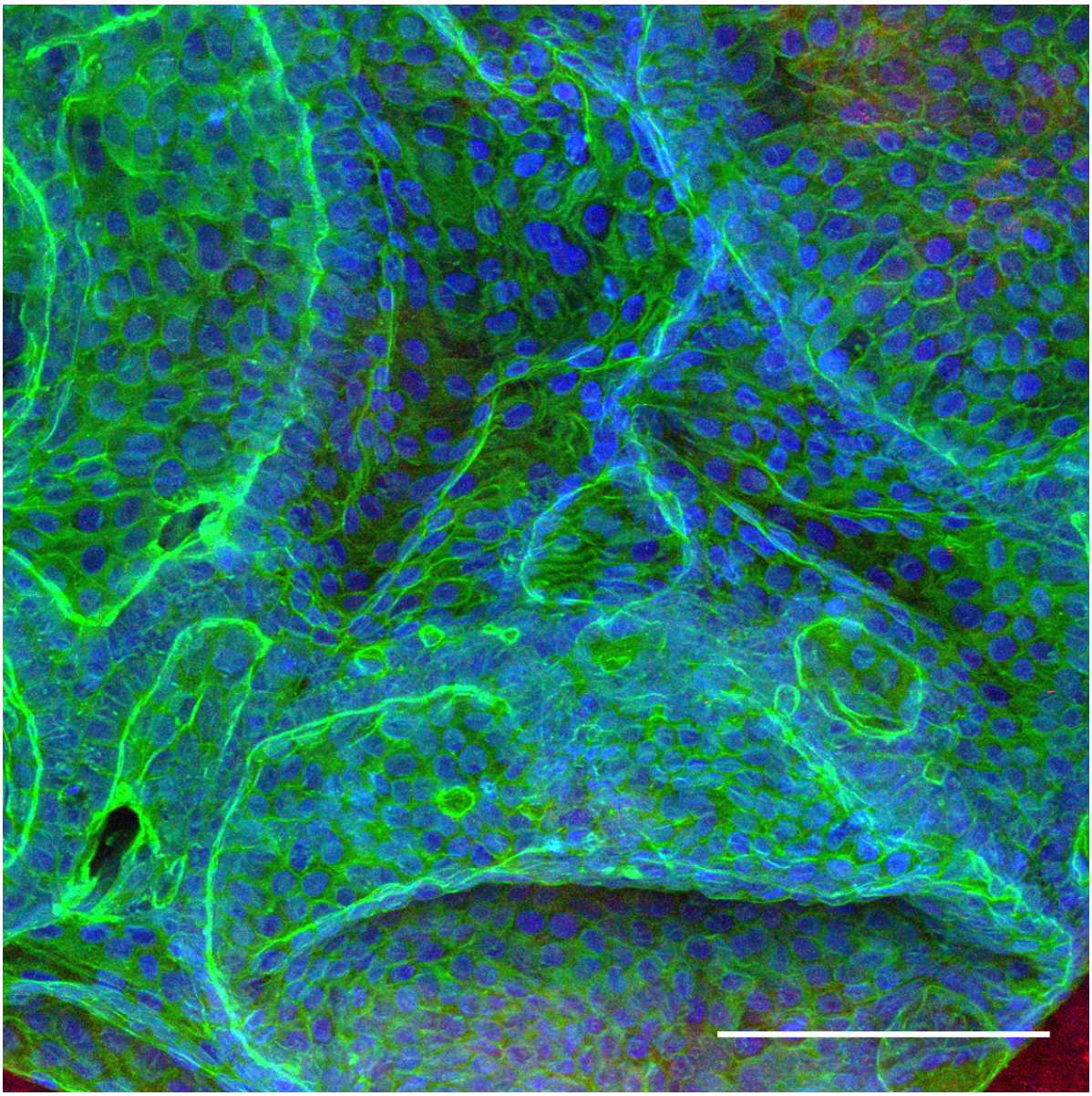

Figure 3.9: Confocal microscopy to evaluate morphology of cells. Close-up merged confocal image of cell nuclei (blue), actin (green) and collagen 1 (red). CCA-derived cells repopulated on tumor scaffolds. Maximum intensity projection revealed the polygonal shape of the attached CCA-derived cells. Scale bar represents 50 µm.

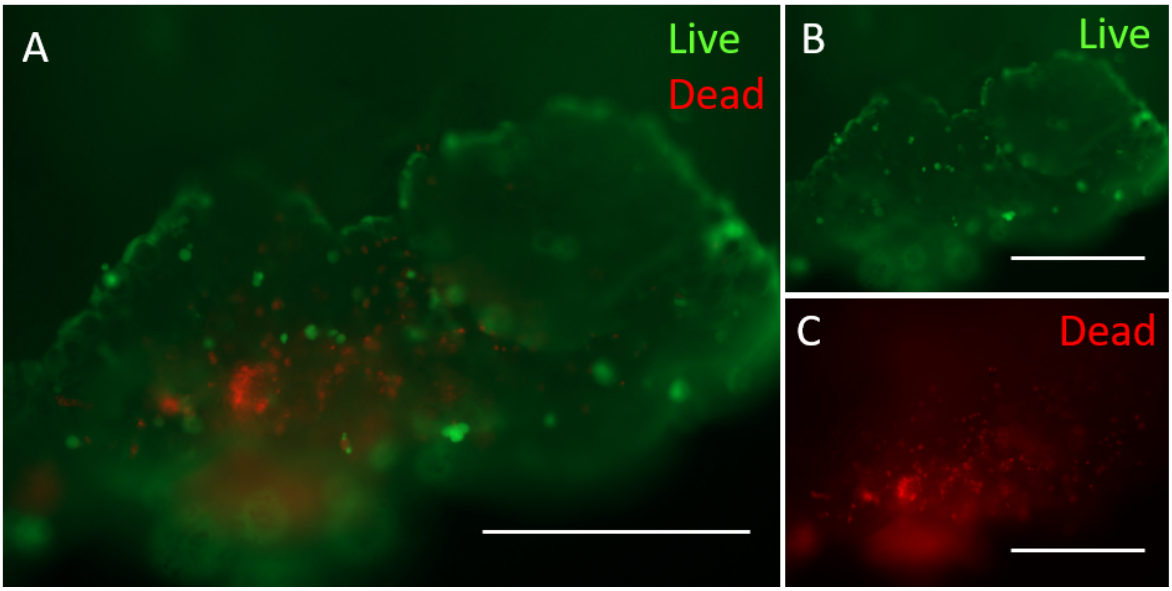

Figure 3.10: Fluorescence images of LIVE/DEAD assay on CCA-derived cells grown on non-tumor scaffold. **(A)** Merged channels, **(B)** live cells and **(C)** dead cells. More viable (green) than dead (red) cells in the recellularized scaffold after 14 days. Scale bars represent 2000 µm.

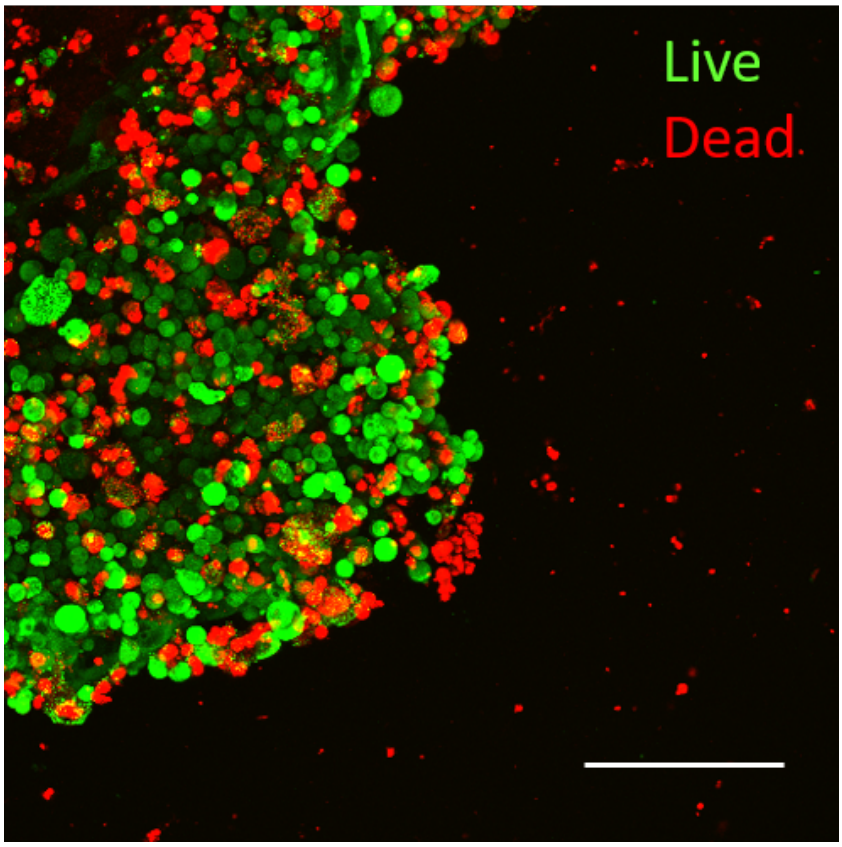

Figure 3.11: Confocal maximum intensity projection image of LIVE/DEAD assay on CCA-derived cells grown in non-tumor scaffold. Viable (green) and dead cells (red) were observed in the recellularized scaffold after 14 days of culture. Scale bar represents 100 µm.

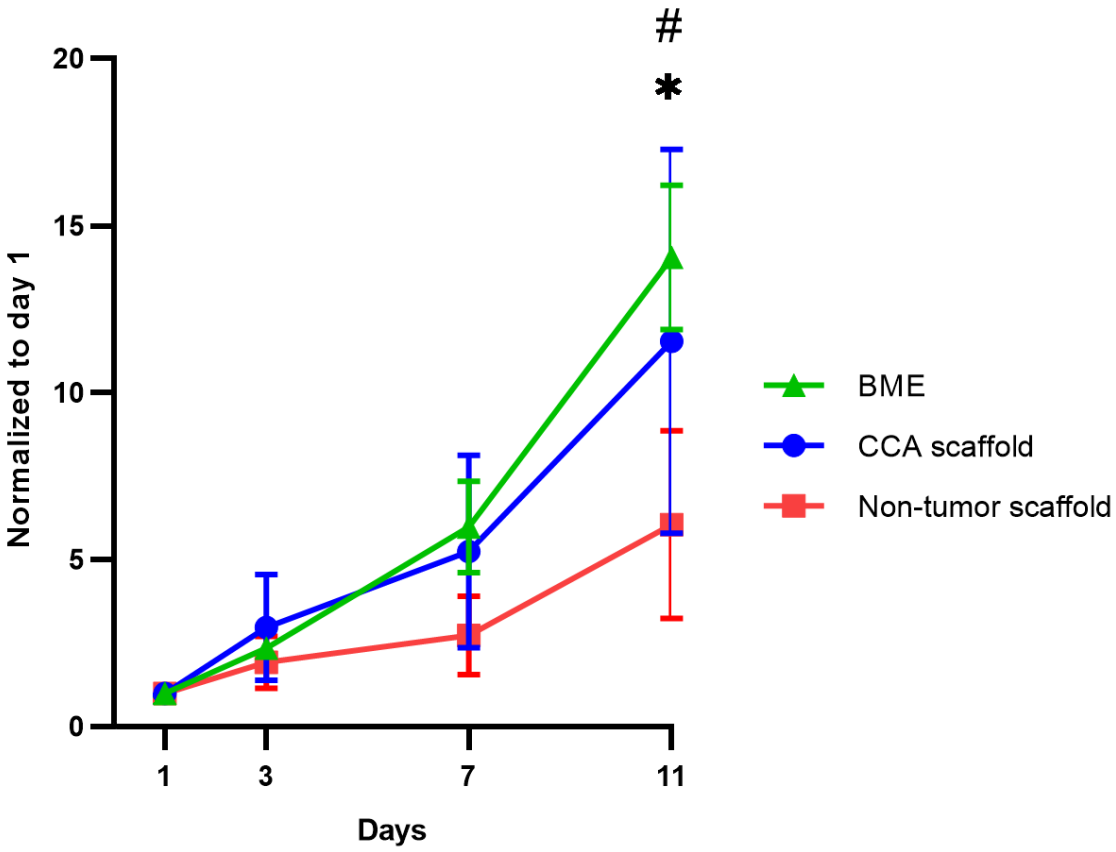

Figure 3.12: Increasing metabolic activity of the engineered tissue during 11 days measured by Presto Blue Assay. Metabolic activity of CCA-derived organoids reseeded in a CCA-scaffold, in non-tumor scaffold and in BME. Data is normalized to day 1. Significant differences regarding metabolic activity were found at day 11 between the cells seeded in CCA scaffold and cells seeded in normal liver scaffolds. A-cellular scaffolds were reseeded with 100.000 cells per CCA-tumor scaffold or normal liver scaffold and with 25.000 cells in BME. Data is normalized to day 1 to compensate for the difference in number of cells seeded. Day 1 was measured 24 hours after recellularization. Results of Presto Blue Assay on empty scaffolds is subtracted. Metabolic activity of CCA-derived cells of 3 different patients were analyzed in the scaffolds. *significant difference between BME and non-tumor scaffold. # significant difference between CCA scaffold and non-tumor scaffold. Data are expressed as mean ± SD. ANOVA repeated measures ($p<0.05$).

3.2.5. Quantitative gene expression comparison between the scaffolds

To compare the effect of the extracellular matrix scaffolds on gene expression of reseeded CCA cells a quantitative PCR was performed. The expression of genes of CCA-derived cells derived from 3 different patients reseeded in non-tumor scaffold, two different CCA scaffolds and in BME were compared after 14 days of culture. The data is summarized in Figure 4.13. The gene expression of *Ki67* was analyzed to evaluate whether the scaffolds differently modulated proliferation. Comparison between the scaffolds revealed that *Ki67* expression level was lower in recellularized non-tumor and CCA 2 scaffold compared with BME, suggesting a lower proliferation rate of cells grown in the ECM scaffolds. Gene expression of stem cell markers, *LGR5*, *CD44*, *CD13*, *CD133*, was not significant different between the scaffolds. *S100A4* gene expression was assessed to estimate the difference in tumor metastasis between the scaffolds. Results indicate a significant higher expression of *S100A4* in cells grown in BME compared to the cells reseeded in the a-cellular scaffolds. Cells seeded in BME expressed significantly more tumor suppressor gene *TP53* than cells seeded in ECM scaffolds. No differences were observed in gene expression of *N-cad*, *E-cad* and *Vimentin*, genes playing a role in cell-cell adhesion and epithelial to mesenchymal transition (EMT) related to metastasis.

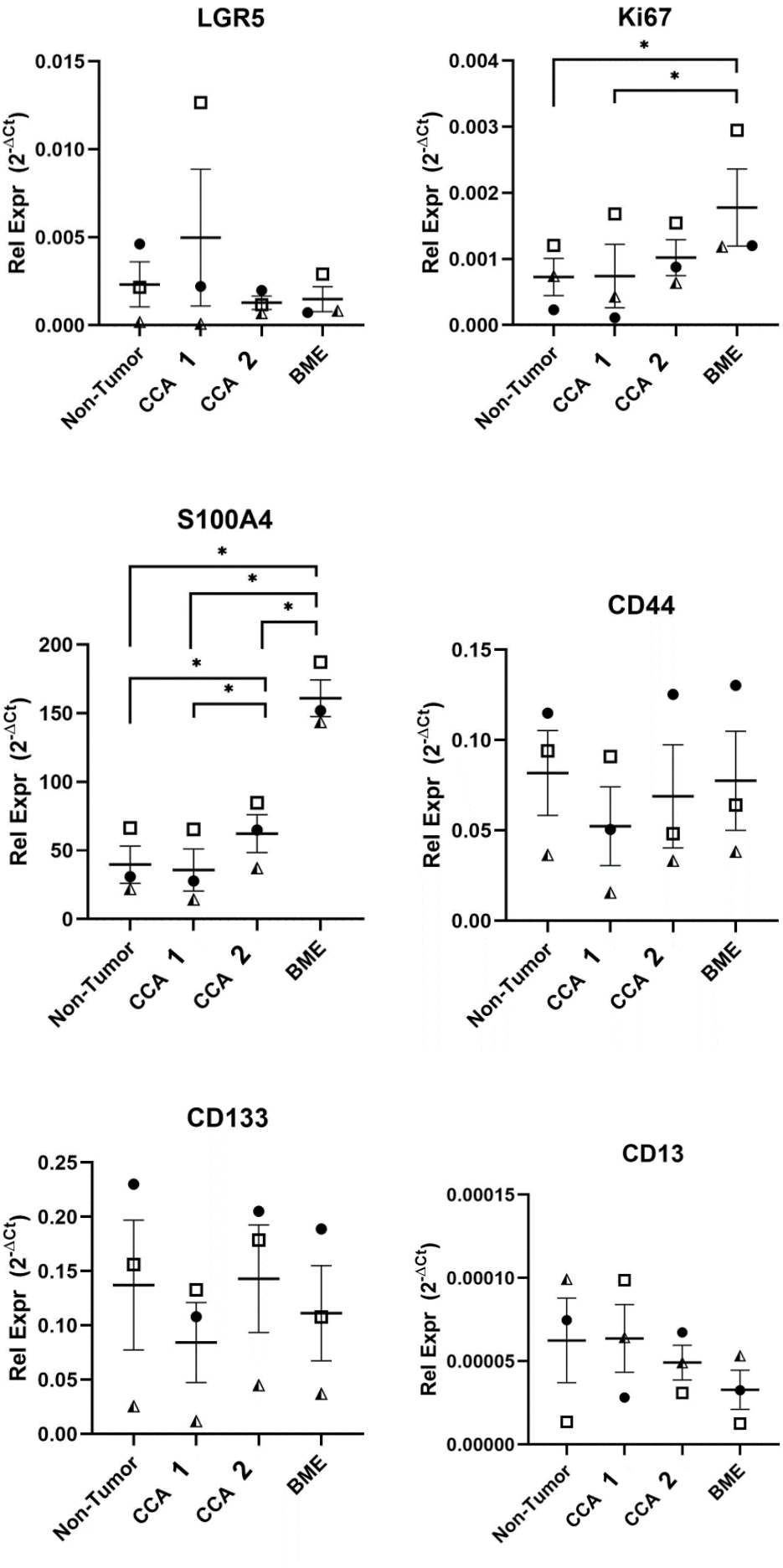
LGR5
Rel Expr (2^-ΔCt)
0.015
0.010
0.005
0.000
Non-Tumor
CCA 1
CCA 2
BME
Ki67
Rel Expr (2^-ΔCt)
0.004
0.003
0.002
0.001
0.000
*
*
Non-Tumor
CCA 1
CCA 2
BME
S100A4
Rel Expr (2^-ΔCt)
200
150
100
50
0
*
*
*
*
*
Non-Tumor
CCA 1
CCA 2
BME
CD44
Rel Expr (2^-ΔCt)
0.15
0.10
0.05
0.00
Non-Tumor
CCA 1
CCA 2
BME
CD133
Rel Expr (2^-ΔCt)
0.25
0.20
0.15
0.10
0.05
0.00
Non-Tumor
CCA 1
CCA 2
BME
CD13
Rel Expr (2^-ΔCt)
0.00015
0.00010
0.00005
0.00000
Non-Tumor
CCA 1
CCA 2
BME

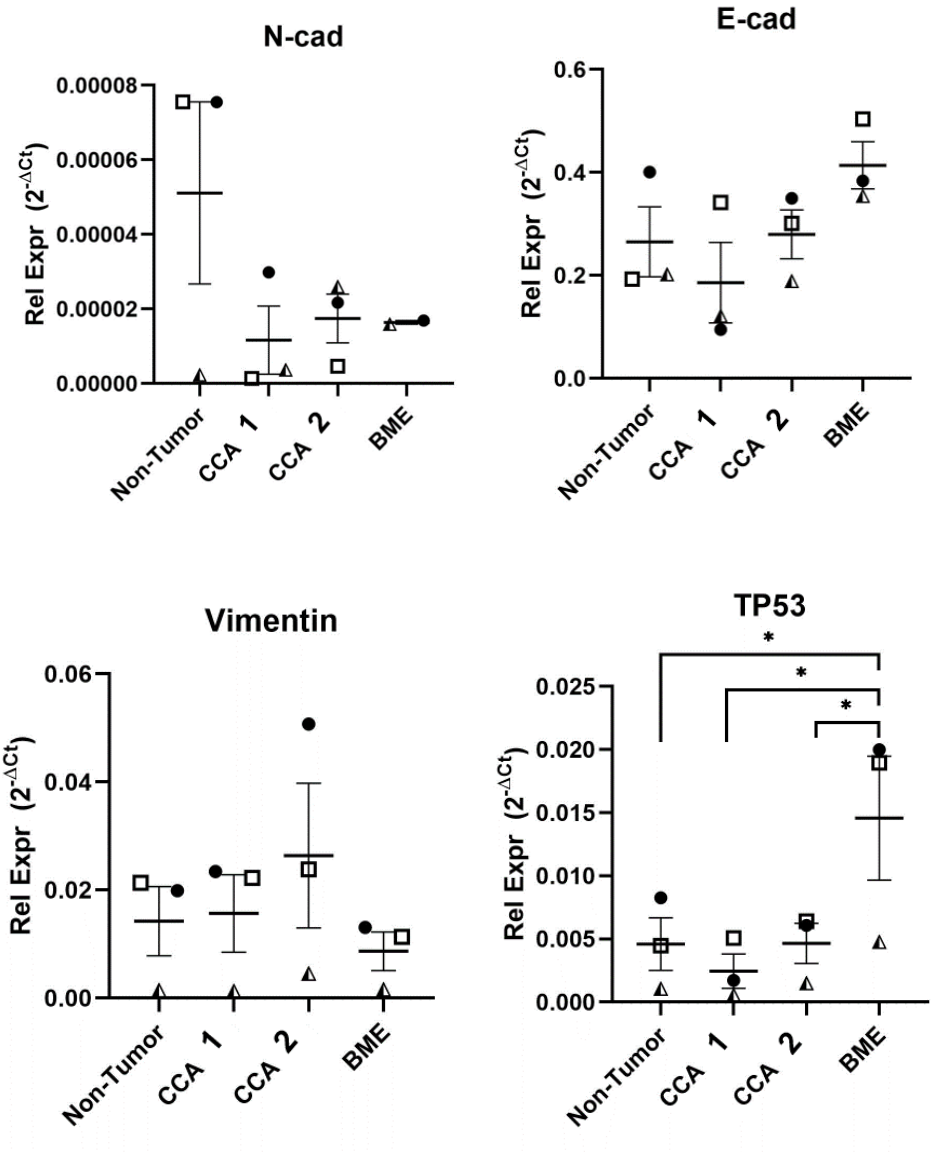

Figure 4.13: Results of quantitative real time PCR. mRNA expression of stem cell marker (LGR5, CD13, CD44, CD133), proliferation (Ki67) EMT related (E-cad, N-cad, Vimentin) and chemoresistance related (TP53) gene evaluation by quantitative real-time PCR. Gene expression data were normalized to the housekeeping genes. Comparison between 4 different matrices (Non-tumor, CCA 1, CCA 2 and BME) is made which were all populated with CCA cells derived from 3 different patients, each represented by their own symbol. Data are expressed as mean ±SD. One-way ANOVA (*$p < 0.05$).

4

Discussion

The great clinical impact of CCA is mainly due to the high chemoresistance observed in patients. An *in vitro* tumor model closely mimicking the original patients tumor could uncover underlying mechanisms in chemo-resistance and enable personalized drug testing. Several components of the tumor niche, both non-cellular and cellular are known to be involved in chemoresistance in CCA. It is therefore urgent to develop a culture platform including the native tumor extracellular matrix. In the present study, we successfully established a protocol to obtain ECM from CCA tumors via decellularization. The obtained matrix served as a scaffold for CCA-derived organoids.

4.1. Decellularization protocol

This study shows that small tumor scaffolds can be derived by decellularization without perfusion through the vascular system. The used protocol was based on the study of *Mazza et al., 2017* who used a protocol to decellularize small liver cubes by employing high shear stress in small volumes of detergents. Here, we adapted the protocol to higher volumes and low shear stress. While most decellularization protocols use sodium dodecyl sulfate (SDS) or sodium deoxycholate (SDC), detergents which are shown to damage or remove ECM components [24, 30], here we only use the mild detergent Triton X-100. Histologic examination after decellularization showed successful removal of cells. However, quantification of DNA content revealed 62.3 ng/mg DNA remained in the tissue, a reduction of 88%, which is close to but still above the accepted 50 ng/mg values proposed by colleagues in the field [31]. Remaining DNA-fragments should be further bio-analyzed to determine the detectability of double stranded DNA. For further optimization of the protocol to generate cell-free scaffold without the use of SDS or SDC, development of a method to perfuse small biopsies, without intact vascular system, is recommended. This could also offer a solution to the elimination of fat in the non-tumor tissue biopsies, which we could not successfully decellularize using the biopsy decellularization protocol due to the high fat content of livers discarded for transplantation. However, the whole organ perfusion protocol to decellularize normal liver elaborated in our lab makes use of the same detergents which enabled the comparison between tumor and normal liver tissue.

4.2. Characterization of ECM in tumor and normal liver tissue

The decellularization of tumor tissue not only creates a scaffold but also enables to characterize the precise composition of ECM without cells. Imaging collagen 1 and 3 in decellularized tissue elucidated the effect of tumor ingrowth on ECM composition. In tumor scaffolds, the collagen fibers were more dense, heterogeneous and disorganized compared to normal liver tissue, which resembles the native tissue morphology differences between tumor and normal tissue [4, 32]. It is recom-

mended to further determine ECM protein composition by proteomic analysis and glycosaminoglycans (GAG) quantification, and to evaluate the ECM structure by scanning electron microscopy.

Collagen is well known to give stiffness to tissues. Since a higher collagen density was found in tumor tissue, we expect a higher stiffness of tumor tissue as compared to normal liver tissue. In literature, CCA tumor tissue was not yet biomechanically measured but only assumed stiffer because of elevated expression of YAP and TAZ, sensors directly regulated by ECM stiffness [4, 33]. Here, the biomechanical properties of CCA tissue were determined on nanoscale using a nanoindentation device. Measurements on normal liver tissue have been performed in our lab with the same device. The Young's Modulus of fresh CCA tissue was 3 times higher compared to reported stiffness for normal liver tissue [27], confirming the stiffening of the tumor extracellular matrix upon tumor ingrowth. The results are in line with previous studies on mammary gland, colon and breast cancer [32, 34]. A high standard deviation of the measurements revealed the high biomechanical heterogeneity of the tissues on nanoscale. Decellularization did not significantly affect stiffness of the tissue. However, a large number of measurements is needed in future research to confirm the preservation of biomechanical properties. Since ECM composition and biomechanical properties of the micro-environment influence cell behavior we hypothesized difference in metabolic activity and gene expression between tumor, non-tumor and the standard BME culture [35, 36]. To this aim the decellularized tissues were repopulated with CCA-derived organoids.

4.3. Difference in cell behavior between scaffolds

The recellularization with CCA-derived organoids showed viable cells inside the a-cellular scaffolds after 14 days. Cells were metabolic active and genes related to stemness, proliferation and tumor metastasis were expressed. The standard culture in BME hydrogel, consisting of tumor matrix membrane matrix produced by mouse sarcoma cells, is known to maintain stemness of cells and prevent differentiation [37]. Cells grown in tumor scaffolds and BME showed higher metabolic activity as compared to non-tumor matrix, suggesting higher proliferation rates in scaffolds containing tumor matrix. In contrast, we do not report differences in gene expression levels of stem cell marker LGR5. Here, we do report higher TP53 and S100A4 expression in BME as compared with the a-cellular scaffolds. TP53 is a tumor suppressor gene whereas S100A4 alterations are linked to tumor metastasis [38]. The differences in gene expression elucidates the importance of the selection of the niche in which the cells are cultures. The lack of specific CCA markers limits the evaluation of the tumorigenicity of the culture [13]. To further study cell-to-matrix interactions, cells grown in liver ECM or ECM obtained from CCA tumors should be compared in terms of proliferation rates, cell migration and matrix invasion.

4.4. Future perspectives

The results of this study provide a base for recreating the native tumor micro-environment *in vitro* which can ultimately be used to study the effectiveness of anti-fibrotic therapeutics targeting the ECM in combination with chemotherapy. The necessity of including not only the non-cellular, but also the cellular components of the tumor stroma is of great importance to create a complete tumor micro-environment [4]. For this the engineered scaffold could be co-cultured with the tumor associated stromal cells, playing an important role in ECM rearrangement [4] and other stromal cells. Moreover, the scaffolds produced here could directly be used in a tumor-on-a-chip system to enhance cellular distribution in the scaffold and to improve oxygenation of the tissue [23]. Oxygenation and delivery of nutrients could reduce cellular death in the core of the tissues. Timescale of decellularization protocol and establishment of the organoids make the culture system suitable for personal medicine approaches. The complete culture platform may enable the identification of drug-sensitivity of patient-specific tumor cells.

5

Conclusion

In this study, the decellularization protocol without perfusion through the vascular system is effective to obtain cell-free extracellular matrix of cholangiocarcinoma tissue. Cells are removed from the tissue and the extracellular matrix preserved the original collagen structure. Compared to normal liver tissue, the collagen fibers of tumor tissue were more dense, heterogeneous and disorganized confirming the importance to distinguish between the tissues. Here we prove that the obtained extracellular matrix can be used as a scaffold for tumor engineering purposes. CCA-derived organoids are a promising cell source as the engrafted cells were viable and were metabolic active. Although tumor scaffolds were denser and stiffer as compared to normal liver scaffolds this did not result in a difference in gene expression. Some genes related to tumorigenicity were higher expressed in standard BME cultured compared to the recellularized scaffolds elucidating the importance of the selection of the niche in which cells are cultured. To improve the general knowledge of cell-ECM interactions in tumors, more research is needed to characterize the extracellular matrix and its effect on tumor progression. Altogether, the resulting combination of tumor-derived organoids and native tumor extracellular matrix provide an innovative basis for a model in which chemo-resistance can be studied and its interaction with desmoplasia. For this, future studies should focus on including the cellular component of the tumor stroma in the culture platform.

Acknowledgments

First, I would like to thank my daily supervisor at the Erasmus MC, Monique Verstegen. This thesis would not have been possible without her idea to combine decellularized tumor tissue with tumor organoids. I want to thank her for the daily feedback, everything I have learned from her and providing such a positive environment in and around the lab. I would like to thank Gilles van Tienderen for the collaboration, support and good times in the lab. Luc van der Laan for the opportunity to work in his group and the inspiring discussions. I am thankful for the help I received from Jorke Willemse, who thought me all the ins and outs of decellularization and provided me a decellularized normal liver. Ruby Lieshout and Yik Kan for providing me the established CCA-derived organoids. I would like to thank Lidy Fratila-Apachitei for her supervision and feedback from the TU Delft. Last I would like to thank the members of the graduation committee.

Abbreviations

ANOVA	Analysis of variance
BME	Basement Membrane Matrix
CCA	Cholangiocarcinoma
DAPI	4,6-diamidino-2-phenylindole
dH_2O	Deionized water
ECM	Extracellular matrix
H&E	Haematoxylin and eosin
OCT	Optimal Cutting Temperature
Rpm	Revolutions per minute
RT	Room temperature
PBS	Phosphate-buffered saline
PS	Penicillin-streptomycin
PSR	Picrosirius Red
SD	Standard deviation
SDC	Sodium deoxycholate
SDS	Sodium dodecyl sulfate
SHG	Second harmonic generation

Bibliography

[1] BWKP Stewart, Christopher P Wild, and others. World cancer report. 404. 2014.

[2] JRA Skipworth, SWM Olde Damink, C Imber, J Bridgewater, SP Pereira, and M Malagó. Surgical, neo-adjuvant and adjuvant management strategies in biliary tract cancer. *Alimentary pharmacology & therapeutics*, 34(9):1063–1078, 2011.

[3] Sumera Rizvi and Gregory J Gores. Pathogenesis, diagnosis, and management of cholangiocarcinoma. *Gastroenterology*, 145(6):1215–1229, 2013.

[4] Massimiliano Cadamuro, Tommaso Stecca, Simone Brivio, Valeria Mariotti, Romina Fiorotto, Carlo Spirli, Mario Strazzabosco, and Luca Fabris. The deleterious interplay between tumor epithelia and stroma in cholangiocarcinoma. *Biochimica et Biophysica Acta (BBA)-Molecular Basis of Disease*, 2017.

[5] Golam Kibria, Hiroto Hatakeyama, and Hideyoshi Harashima. Cancer multidrug resistance: mechanisms involved and strategies for circumvention using a drug delivery system. *Archives of pharmacal research*, 37(1):4–15, 2014.

[6] William R Jarnagin, Yuman Fong, Ronald P DeMatteo, Mithat Gonen, Edmund C Burke, Jessica Bodniewicz, Miranda Youssef, David Klimstra, and Leslie H Blumgart. Staging, resectability, and outcome in 225 patients with hilar cholangiocarcinoma. *Annals of surgery*, 234(4):507, 2001.

[7] Juan Valle, Harpreet Wasan, Daniel H Palmer, David Cunningham, Alan Anthoney, Anthony Maraveyas, Srinivasan Madhusudan, Tim Iveson, Sharon Hughes, Stephen P Pereira, et al. Cisplatin plus gemcitabine versus gemcitabine for biliary tract cancer. *New England Journal of Medicine*, 362(14):1273–1281, 2010.

[8] JL Ku, KA Yoon, IJ Kim, WH Kim, JY Jang, KS Suh, SW Kim, YH Park, JH Hwang, YB Yoon, et al. Establishment and characterisation of six human biliary tract cancer cell lines. *British journal of cancer*, 87(2):187, 2002.

[9] Giuliana Cavalloni, Caterina Peraldo-Neia, Chiara Varamo, Laura Casorzo, Carmine Dell'Aglio, Paola Bernabei, Giovanna Chiorino, Massimo Aglietta, and Francesco Leone. Establishment and characterization of a human intrahepatic cholangiocarcinoma cell line derived from an italian patient. *Tumor Biology*, 37(3):4041–4052, 2016.

[10] Jorke Willemse, Ruby Lieshout, Luc JW van der Laan, and Monique MA Verstegen. From organoids to organs: Bioengineering liver grafts from hepatic stem cells and matrix. *Best Practice & Research Clinical Gastroenterology*, 31(2):151–159, 2017.

[11] Laura Broutier, Gianmarco Mastrogiovanni, Monique MA Verstegen, Hayley E Francies, Lena Morrill Gavarró, Charles R Bradshaw, George E Allen, Robert Arnes-Benito, Olga Sidorova, Marcia P Gaspersz, et al. Human primary liver cancer–derived organoid cultures for disease modeling and drug screening. *Nature medicine*, 23(12):1424, 2017.

[12] Meritxell Huch, Helmuth Gehart, Ruben van Boxtel, Karien Hamer, Francis Blokzijl, Monique MA Verstegen, Ewa Ellis, Martien van Wenum, Sabine A Fuchs, Joep de Ligt, et al. Long-term culture of genome-stable bipotent stem cells from adult human liver. *Cell*, 160(1-2):299–312, 2015.

[13] Silvestre Vicent, Ruby Lieshout, Anna Saborowski, Monique MA Verstegen, Chiara Raggi, Stefania Recalcati, Pietro Invernizzi, Luc JW van der Laan, Domenico Alvaro, Diego F Calvisi, et al. Experimental models to unravel the molecular pathogenesis, cell of origin and stem cell properties of cholangiocarcinoma. *Liver International*, 39:79–97, 2019.

[14] Manel Esteller. Epigenetic changes in cancer. *F1000 biology reports*, 3, 2011.

[15] Masako Ochiai, Yasunori Yoshihara, Yoshiaki Maru, Tetsuya Matsuura, Masashi Izumiya, Toshio Imai, and Yoshitaka Hippo. Kras-driven heterotopic tumor development from hepatobiliary organoids. *Carcinogenesis*, 2019.

[16] Vassilis Papalazarou, Manuel Salmeron-Sanchez, and Laura M Machesky. Tissue engineering the cancer microenvironment—challenges and opportunities. *Biophysical reviews*, pages 1–17, 2018.

[17] Simone Brivio, Massimiliano Cadamuro, Mario Strazzabosco, and Luca Fabris. Tumor reactive stroma in cholangiocarcinoma: The fuel behind cancer aggressiveness. *World journal of hepatology*, 9(9):455, 2017.

[18] Johanna A Joyce and Douglas T Fearon. T cell exclusion, immune privilege, and the tumor microenvironment. *Science*, 348(6230):74–80, 2015.

[19] Claudia Mazio, Costantino Casale, Giorgia Imparato, Francesco Urciuolo, and Paolo Antonio Netti. Recapitulating spatiotemporal tumor heterogeneity in vitro through engineered breast cancer microtissues. *Acta biomaterialia*, 73:236–249, 2018.

[20] Georg Halder, Sirio Dupont, and Stefano Piccolo. Transduction of mechanical and cytoskeletal cues by yap and taz. *Nature reviews Molecular cell biology*, 13(9):591, 2012.

[21] Mina J Bissell and William C Hines. Why don't we get more cancer? a proposed role of the microenvironment in restraining cancer progression. *Nature medicine*, 17(3):320, 2011.

[22] Mónica Romero-López, Andrew L Trinh, Agua Sobrino, Michaela MS Hatch, Mark T Keating, Cristhian Fimbres, David E Lewis, Paul D Gershon, Elliot L Botvinick, Michelle Digman, et al. Recapitulating the human tumor microenvironment: colon tumor-derived extracellular matrix promotes angiogenesis and tumor cell growth. *Biomaterials*, 116:118–129, 2017.

[23] Giuseppe Mazza, Walid Al-Akkad, Andrea Telese, Lisa Longato, Luca Urbani, Benjamin Robinson, Andrew Hall, Kenny Kong, Luca Frenguelli, Giusi Marrone, et al. Rapid production of human liver scaffolds for functional tissue engineering by high shear stress oscillation-decellularization. *Scientific reports*, 7(1):5534, 2017.

[24] Monique MA Verstegen, Jorke Willemse, Sjoerd van den Hoek, Gert-Jan Kremers, Theo M Luider, Nick A van Huizen, Francois EJA Willemssen, Herold J Metselaar, Jan NM IJzermans, Luc JW van der Laan, et al. Decellularization of whole human liver grafts using controlled perfusion for transplantable organ bioscaffolds. *Stem cells and development*, 26(18):1304–1315, 2017.

[25] Basak E Uygun, Alejandro Soto-Gutierrez, Hiroshi Yagi, Maria-Louisa Izamis, Maria A Guzzardi, Carley Shulman, Jack Milwid, Naoya Kobayashi, Arno Tilles, Francois Berthiaume, et al. Organ reengineering through development of a transplantable recellularized liver graft using decellularized liver matrix. *Nature medicine*, 16(7):814, 2010.

[26] Thomas Shupe, Matthew Williams, Alicia Brown, Bradley Willenberg, and Bryon E Petersen. Method for the decellularization of intact rat liver. *Organogenesis*, 6(2):134–136, 2010.

[27] Jorke Willemse, Monique MA Verstegen, Annewiet Vermeulen, Ivo Schurink, Henk P Roest, Luc JW van der Laan, and Jeroen de Jonge. Fast, robust and effective decellularization of whole human livers using mild detergents and pressure controlled perfusion. *Materials Science and Engineering: C*, page 110200, 2019.

[28] Giorgio Mattei, G Gruca, N Rijnveld, and ARTI Ahluwalia. The nano-epsilon dot method for strain rate viscoelastic characterisation of soft biomaterials by spherical nano-indentation. *Journal of the mechanical behavior of biomedical materials*, 50:150–159, 2015.

[29] Jo Vandesompele, Katleen De Preter, Filip Pattyn, Bruce Poppe, Nadine Van Roy, Anne De Paepe, and Frank Speleman. Accurate normalization of real-time quantitative rt-pcr data by geometric averaging of multiple internal control genes. *Genome biology*, 3(7):research0034–1, 2002.

[30] Thomas W Gilbert. Strategies for tissue and organ decellularization. *Journal of cellular biochemistry*, 113(7):2217–2222, 2012.

[31] Peter M Crapo, Thomas W Gilbert, and Stephen F Badylak. An overview of tissue and whole organ decellularization processes. *Biomaterials*, 32(12):3233–3243, 2011.

[32] ML Pinto, E Rios, AC Silva, SC Neves, HR Caires, AT Pinto, C Duraes, FA Carvalho, AP Cardoso, NC Santos, et al. Decellularized human colorectal cancer matrices polarize macrophages towards an anti-inflammatory phenotype promoting cancer cell invasion via ccl18. *Biomaterials*, 124:211–224, 2017.

[33] Francesca Zanconato, Michelangelo Cordenonsi, and Stefano Piccolo. Yap/taz at the roots of cancer. *Cancer cell*, 29(6):783–803, 2016.

[34] Victoria Seewaldt. Ecm stiffness paves the way for tumor cells. *Nature medicine*, 20(4):332, 2014.

[35] Sirio Dupont, Leonardo Morsut, Mariaceleste Aragona, Elena Enzo, Stefano Giulitti, Michelangelo Cordenonsi, Francesca Zanconato, Jimmy Le Digabel, Mattia Forcato, Silvio Bicciato, et al. Role of yap/taz in mechanotransduction. *Nature*, 474(7350):179, 2011.

[36] Amit Pathak and Sanjay Kumar. Transforming potential and matrix stiffness co-regulate confinement sensitivity of tumor cell migration. *Integrative Biology*, 5(8):1067–1075, 2013.

[37] Slobodan Vukicevic, Hynda K Kleinman, Frank P Luyten, Anita B Roberts, Nanette S Roche, and A Hari Reddi. Identification of multiple active growth factors in basement membrane matrigel suggests caution in interpretation of cellular activity related to extracellular matrix components. *Experimental cell research*, 202(1):1–8, 1992.

[38] Jose Luis Hernandez, Laura Padilla, Sheila Dakhel, Toni Coll, Rosa Hervas, Jaume Adan, Marc Masa, Francesc Mitjans, Josep Maria Martinez, Silvia Coma, et al. Therapeutic targeting of tumor growth and angiogenesis with a novel anti-s100a4 monoclonal antibody. *PloS one*, 8(9):e72480, 2013.

Supplementary Material

Supplemental Figures

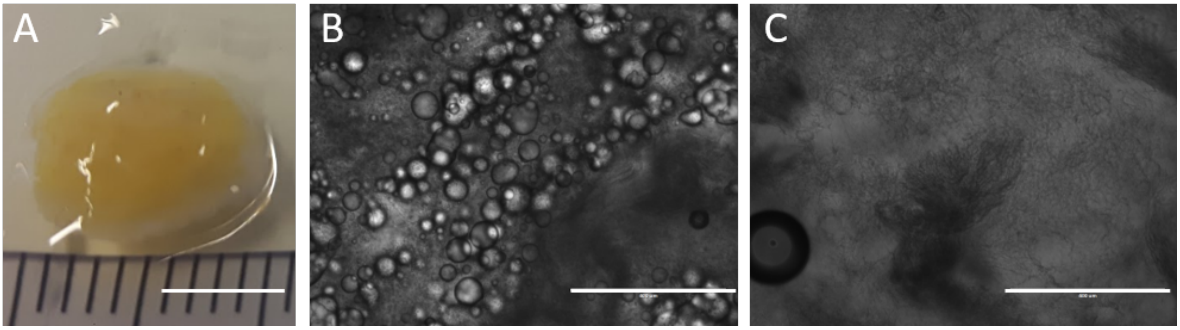

Figure S1: Normal liver decellularization using the decellularization protocol for small biopsies. **(A)** Normal liver tissue looked macroscopically yellow/brownish after decellularization, scale bar represents 5 mm. **(B)** Fat droplets were visible using brightfield microscopy in the decellularized normal tissue. Scale bar represents 400 µm. **(C)**. After isopropanol treatment the amount of fat was reduced visualized by brightfield microscopy. Scale bar represents 400 µm.

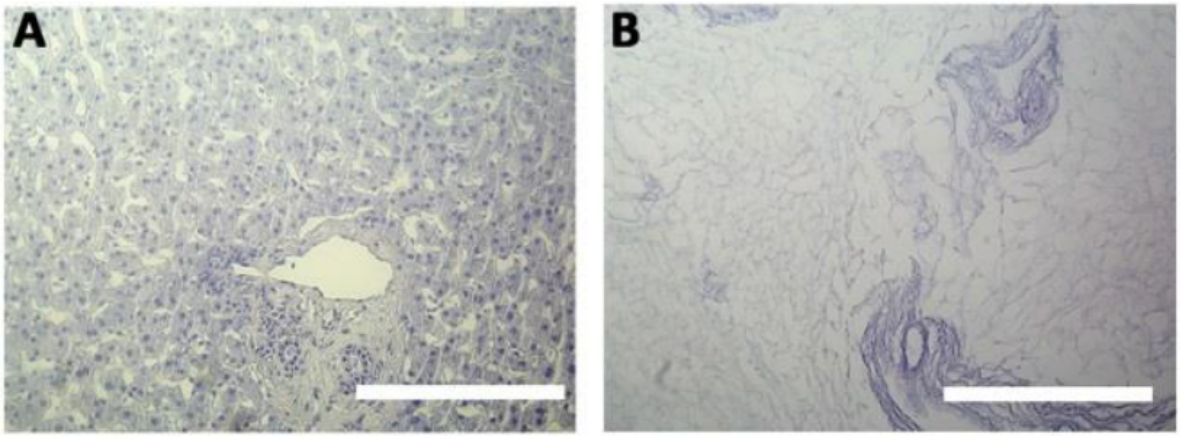

Figure S2: Normal liver decellularization using whole organ decellularization perfusion. **(A)** Fresh and **(B)** decellularized. H&E staining confirmed the removal of cells after decellularization using whole organ perfusion. Scale bars represent 100 µm. Images are originating from a paper submitted for publishing (Willemse et al., 2019) [27].

Supplemental Tables

Table S1: Components and concentrations of Expansion Medium

Component	**Concentration**
DMEM /F12	Base medium
Primocin	50 µg/ml
Ultraglutamine	1%
HEPES	10 mM
B27 supplement (without Vitamin A)	1:50
N2 supplement	1:100
N-Acetyl-L-cysteine	1.25 mM
Rspo-1 conditioned medium	10%
Nicotinamide	10 mM
Recombinant human [Leu15]-Gastrin I	10 nM
Recombinant human EGF	50 ng/ml
Recombinant human FGF10	100 ng/ml
Recombinant human HGF	25 ng/ml
Forskolin	10 µM
A8301	5 µM

Table S2: Used primers

	Forward primer	**Reverse primer**
GAPDH	CTTTTGCGTCGCCAGCCGAG	CCAGGCGCCCAATACGACCA
B2M	GTGTCTGGGTTTCATCCATC	GGCAGGCATACTCATCTTTT
CD13	CAGTGACACGACGATTCTCC	CCTGTTTCCTCGTTGTCCTT
CD44	TGCCGCTTTGCAGGTGTAT	GGCCTCCGTCCGAGAGA
CD133	CCTGGGGCTGCTGTTTATTA	ATCACCAACAGGGAGATTGC
Vimentin	CGGGAGAAATTGCAGGAGG	TGCTGTTCCTGAATCTGAGC
TP53	GAGCGTGCTTTCCACGAC	TGTTTCCTGACTCAGAGGGG
LGR5	GTCAGCTGCTCCCGAATCCC	TGAAACAGCTTGGGGGCACA
Ki67	CTACGGATTATACCTGGCCTTCC	AGGAAGCTGGATACGGATGTCA
S100A4	GGCAGGGAGGGTGACAAGCA	CCTCCTGGTCCTTGTTCCGGT
N-cad	AGTCAACTGCAACCGTGTCT	AGCGTTCCTGTTCCACTCAT
E-cad	CTGGACAGGGAGGATTTTGA	ACCTGAGGCTTTGGATTCCT